REPORT DOCUMENTATION PAGE

READ INSTRUCTIONS BEFORE COMPLETING FORM

1. REPORT NUMBER: AFFDL-TR-75-132	2. GOVT ACCESSION NO.
3. RECIPIENT'S CATALOG NUMBER	
4. TITLE (and Subtitle): FURTHER INVESTIGATIONS OF THE NEAR FIELD TRAILING VORTICITY BEHIND A STOL AIRCRAFT	5. TYPE OF REPORT & PERIOD COVERED: Final Report 1 April 74 - 31 December 75
	6. PERFORMING ORG. REPORT NUMBER: AASE 75-142
7. AUTHOR(s): Lawrence J. Mertaugh, Krishna Devarayalu	8. CONTRACT OR GRANT NUMBER(s): F33615-74-C-3066
9. PERFORMING ORGANIZATION NAME AND ADDRESS: Mississippi State University, Aerophysics and Aerospace Eng., P. O. Drawer A, Mississippi State, MS 39762	10. PROGRAM ELEMENT, PROJECT, TASK AREA & WORK UNIT NUMBERS: 19290317
11. CONTROLLING OFFICE NAME AND ADDRESS: Air Force Flight Dynamics Laboratory, Air Force Systems Command, Wright-Patterson AFB, Ohio	12. REPORT DATE: December 1975
	13. NUMBER OF PAGES: 49
14. MONITORING AGENCY NAME & ADDRESS (if different from Controlling Office)	15. SECURITY CLASS. (of this report): UNCLASSIFIED
	15a. DECLASSIFICATION/DOWNGRADING SCHEDULE

16. DISTRIBUTION STATEMENT (of this Report)

Approved for Public Release; Distribution Unlimited

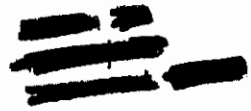

17. DISTRIBUTION STATEMENT (of the abstract entered in Block 20, if different from Report)

18. SUPPLEMENTARY NOTES

19. KEY WORDS (Continue on reverse side if necessary and identify by block number)

Wake	Ground Effect	Anemometer
Vortex	Span Load	Instrumentation
Trailing Vortex	STOL Aircraft	
Flight Test	Flow Visualization	

20. ABSTRACT (Continue on reverse side if necessary and identify by block number)

This report presents the results of a test program to measure the velocity field in the near-wake behind the wing of a high-lift test aircraft. This research program was a continuation of the flight test measurement program described in Reference 1. A direct measurement of the 3-component velocity vectors was made in several measurement planes located at various longitudinal positions behind the trailing edge of the aircraft wing. The test aircraft was a STOL L-19 equipped with a

distributed suction boundary layer control system. Measurements were taken during this program such that the velocity derivatives along all three coordinate axes could be computed. Thus, the three components of the vorticity vector could be determined at each point of the measurement matrix. It was found that, in general, the velocity and vorticity vectors are not collateral.

A design study was conducted to determine the feasibility of a trailing probe support system which would allow detailed mapping of the wing wake velocity field at least 4 chord lengths behind the trailing edge of the generating wing. This analysis demonstrates good stability characteristics and a reasonable control system. It is concluded that such a system is feasible and would provide a mechanism for further experimental study of the vortical flow at a point in the wake where the roll-up is more developed.

[redacted]

TABLE OF CONTENTS

LIST OF ILLUSTRATIONS

LIST OF ILLUSTRATIONS (CONCLUDED)

LIST OF TABLES

LIST OF SYMBOLS

b	wing span of the aircraft, feet
C	mean aerodynamic chord of aircraft wing, feet
C_T	tip chord of aircraft wing, feet
C_t	mean aerodynamic chord of trailing wing, feet
C_D	coefficient of drag of the aircraft
C_d	coefficient of drag of the trailing wing system
C_L	coefficient of lift of the aircraft
C_{L_T}	trimmed lift coefficient of aircraft
C_R	coefficient of the trailing-wing vertical load acting on the aircraft and root chord of aircraft wing
C_{D_α}	drag-curve slope of aircraft
C_{L_α}	lift-curve slope of aircraft
$C_{L_{\dot{\alpha}}}$	variation of C_L with $\dot{\alpha}$
C_{L_δ}	variation of C_L with deflection of trailing-wing system
$C_{L_{\dot{\delta}}}$	variation of C_L with $\dot{\delta}$
C_M	pitching moment coefficient about the aircraft center of gravity
C_{M_θ}	variation of C_M with θ
$C_{M_{\dot{\theta}}}$	variation of C_M with $\dot{\theta}$
C_{M_α}	variation of C_M with the aircraft angle of attack
$C_{M_{\dot{\alpha}}}$	variation of C_M with $\dot{\alpha}$
C_{M_δ}	variation of C_M with δ
C_{ℓ_α}	variation of the trailing-wing lift coefficient with α

LIST OF SYMBOLS (Continued)

$C_{\ell_{\dot{\alpha}}}$	variation of trailing wing C_ℓ with $\dot{\alpha}$
C_{ℓ_δ}	variation of trailing wing C_ℓ with deflection of trailing wing system
$C_{\ell_{\dot{\delta}}}$	variation of trailing wing C_ℓ with $\dot{\delta}$
$C_{\ell_{\dot{\theta}}}$	variation of trailing wing C_ℓ with $\dot{\theta}$
$C_{\ell u}$	variation of trailing wing C_ℓ with u
D_t	trailing-wing system drag, pounds
e_t	trailing wing system's radius of gyration, feet
K_y	airplane's radius of gyration about the Y axis, feet
m	mass of airplane excluding the trailing wing system, slugs
m_t	mass of trailing-wing system, slugs
h	$2K_y^2/(\mu C^2)$ $(\mu = m/\rho SC)$
h_1	$2\mu_t X_t/(\mu C)(\mu_t = m_t/\rho S_t C_t)$
h_2	$2\mu_t e_t^2/(\mu^2 C^2)$
L_t	lift of trailing wing, pounds
ℓ_1	$2\mu_t x_t \ell_t/(\mu^2 C^2)$
ℓ_t	distance from c.g. of aircraft to hinge of trailing-wing system, feet
S	wing area of aircraft, square feet
S_t	area of the trailing wing, square feet
U	flight velocity of aircraft, miles per hour or feet per second
V	forward velocity of aircraft, feet per second
X_t	distance from axis of rotation of trailing wing system (Y'Y') to its c.g., feet

LIST OF SYMBOLS (Continued)

u	$\Delta V/V$
u, v, w	velocity components of wing wake, feet per second
u_1	$ue^{-\lambda(t/\tau)}$
α_1	$\alpha e^{-\lambda(t/\tau)}$, (rad.)
δ_1	$\delta e^{-\lambda(t/\tau)}$, (rad.)
θ	angle between the velocity and vorticity vector in wing wake, degrees
θ_1	$\theta e^{-\lambda(t/\tau)}$, (rad.)
$\dot{\alpha}$	variation of α with (t/τ)
$\dot{\delta}$	variation of δ with (t/τ)
$\dot{\theta}$	variation of θ with (t/τ)
ρ	standard sea level density of air (0.002378 slugs per ft^3)
τ	airplane time characteristic $(m/\rho SV)$
λ	real or complex constant of equal value for each independent variable
$\zeta_x, \zeta_y, \zeta_z$	components of vorticity, 1/seconds

Section I

Introduction

A significant effort has been put forth by various private and governmental research organizations to provide a better understanding of the trailing vortex and, if possible, some control over the formation of trailing vorticies. Equipment has been developed which can identify the positions of vortices that are in the vicinity of airports, devices have been tested that appear to affect some reduction in concentrated vorticity when mounted on the generating aircraft and envelopes are being defined that may allow the most likely areas for vortex encounters to be avoided. These achievements promise a means by which the majority of possible vortex encounters may be avoided, but a thorough assessment of the cost of implementing these approaches has yet to be made. For the most part these efforts represent an attempt to live with the generated vorticity, or to minimize its destructive power, without obtaining much additional knowledge regarding the physics of its formation, transport or eventual dissipation. This approach has been dictated by relatively slow progress in basic vortex research, the immediate need to satisfy operational requirements and the need to cope with the very strong vortices produced by the current generation of "jumbo" jets. The objective of the research program discussed in this report was to provide detailed vorticity measurements in the near-wing wake with the hope that these data will yield an accurate basis for comparison with current theoretical models and a much better understanding of what the vortex roll-up phenomenon actually is.

This research program was a continuation of the flight test measurement program described in Reference 1. The program involved the direct measurement of the full velocity vector throughout large measurement planes located at various distances behind the trailing edge of the wing of a flight test aircraft. The test aircraft was a high-lift L-19 equipped with a distributed suction BLC system. The velocity data were then used to compute the vorticity within these measurement planes. Different flight velocities and flap configurations were used to show the effect of these variables.

The present program differs from the previous effort in that additional data were obtained to allow all components of vorticity to be computed. This was accomplished by using two measurement planes located four inches apart. This small longitudinal separation provided the data needed to compute the longitudinal derivatives of velocity. These derivatives, in conjunction with the spanwise and vertical derivatives, provided the data needed to compute all three components of vorticity. These closely-spaced measurements were only made at the forward location (near the wing trailing edge). Additional measurements, using a single measurement plane, were made at an intermediate longitudinal station to add to the roll-up information that was provided in Reference 1. In

addition to the measurements provided in the present program, a preliminary study was conducted into the feasibility of a trailing-wing probe support structure. This assembly would allow precision wake measurements to be made three to five chord lengths behind the wing trailing edge. This study included a preliminary design and a longitudinal stability analysis of the trailing-wing system.

The forward wake measurements conducted in this test program provided data for an effective measurement plane 7.1 inches behind the trailing edge of the inboard section of the wing. Data were taken at one airspeed (an equivalent airspeed of 60 miles per hour) and two flap deflections (zero degrees and full flap deflection). The full flap data for the forward measurement planes are not provided in this report because of problems with the test aircraft and the instrumentation. The intermediate measurement plane data were obtained at the same two flap deflections and two airspeeds (equivalent airspeeds of approximately 60 and 80 miles per hour). The recurrent instrumentation problems also resulted in the loss of data for 80 miles per hour and full flap deflection.

Section II

Equipment and Instrumentation

1. Test Aircraft

The test aircraft was a high-lift L-19 aircraft that is equipped with a distributed-suction turbulent boundary layer control system. This system allows the aircraft to develop large trimmped lift coefficients and provides a wing wake with a minimum of low-momentum flow. This is the same aircraft that was used in the previous test program (see Reference 1).

The wing geometry of the test aircraft is somewhat different than that of a standard L-19 aircraft. The differences in wing geometry are mostly in the larger leading-edge radius and a modified flap geometry. The pertinent geometry data are listed below. These values have been used, where needed, in the data reduction.

$S = 1.768$ square feet

$b = 36.0$ feet (432.0 inches)

$C_R = 5.43$ feet (65.2 inches)

$C_T = 3.58$ feet (43.0 inches)

Aspect Ratio = 7.33

The original airfoil section on the L-19 wing was a NASA 2412 with a wing incidence of 1.5 degrees at the root and -1.5 degrees at the tip. The propeller diameter is 90 inches and the engine is rated at 213 horsepower. It is estimated that about 30 horsepower is required to drive the boundary layer control system.

The aircraft weight and balance were adjusted during the program to maintain constant values as the equipment was moved or changed. The maximum gross weight was maintained at 2560 pounds with the center of gravity at 40.1 inches aft of the reference station. The average mission fuel consumption was 80 pounds which gave a mean test weight of 2520 pounds with the center of gravity at 40.0 inches. This weight was 10 pounds higher than was used in the previous test program. A weight of 2520 pounds was used for data reduction purposes.

A flight test boom was mounted to the left wingtip of the test aircraft for this program. A self-aligning pitot-static head was attached to the boom. The objective of this installation was to eliminate the need for a position error correction for the aircraft airspeed

system. As it turned out, there was still a position error with this device, and a position error correction was applied to all the appropriate test data. The flight instruments were calibrated during the test program, and instrument corrections were applied to the data.

2. Probe Support Structure

The wake measuring probe was moved throughout the measurement plane by means of a vertical traversing mechanism which mounted to a trolley which moved laterally along the horizontal boom. The general arrangement of the installation is shown in Figure 1. The dimensional details of the measurement planes are shown in Figures 2 and 3.

The mounting of the vertical position sensor and the limit switches on the vertical traversing mechanism (VTM) provided 32 inches of vertical travel of the probe. Shifting the mounting of the VTM to the trolley provided an additional 12 inches of travel below the normal (mid) position. Rotating the VTM with respect to the trolley provided an additional 10 inches of travel above the mid position. This 54 inches of total vertical travel defined the height of the measurement planes. This travel represents a reduction in the measurement plane height compared to the previous test program and was a result of changes in the mounting of the position sensors.

The mounting of the boom structures to the test aircraft was changed from the arrangement used in the previous program to allow a lowering of the measurement plane and to provide a four-inch longitudinal shift between the two "forward" measurement planes without major changes in the support structure. The measurement planes were lowered approximately 12 inches. This was to allow more of the flap wake to be surveyed by the probe for full flap deflections. The four-inch separation of the forward measurement planes was to allow the computation of the longitudinal derivatives of the wake velocity. It was important that the relative positions of these forward measurement planes be closely controlled, and the attachment of the boom structure was designed to allow the four-inch shift with a minimum of adjustment. The mounting of the boom support structure to the aircraft located the two forward measurement planes 5.1 and 9.1 inches aft of the trailing edge of the flap with the flap in the up position. This provided a mean forward position of 7.1 inches (0.59 feet) aft of the flap trailing edge. This position was slightly forward of the forward position used in the previous test program. The aft position of the measurement plane, used in this test program, was 33.3 inches (2.78 feet) aft of the flap trailing edge. This position is essentially midway between the measurement planes used in this previous test program. The lateral travel of the VTM support trolley was a total of 205 inches with position information provided over 196 inches of travel.

3. Instrumentation

The measurement of the flow velocities behind the wing of the test aircraft was accomplished with a commercially available total-vector hot-film anemometer. The sensors of this unit consist of three orthogonal rods with split films mounted on each rod. The dimensions of each rod are such that they fit within a 0.3 inch diameter sphere. The films on the rods have a diameter of 0.006 inch and a sensitive length of 0.08 inch. The rods are made of quartz with platinum films. The six active film elements of the probe provide complete velocity vector definition. Ambient temperature is provided by an integral thermocouple. The probe is provided with a protective shield that incorporates a sonic nozzle. Using an external supply of air, this arrangement allows the original factory calibration to be checked prior to each test flight. The test data obtained from this anemometer included six channels of "velocity" data and one channel of temperature data. The temperature channel was also used to record the probe horizontal position information. These data were recorded on a seven channel tape recorder operating at 7.5 inches per second in the FM mode.

Although the basic instrumentation system used in this test program was similar to that used in the previous program, there were a number of significant changes. These changes were intended to improve the system reliability and to allow the tests to be flown without flight observer. Eliminating the flight observer was considered to be desirable in that it provided much more control over the aircraft weight and balance. Additional control of the aircraft weight and balance is needed for some of the anticipated future research efforts that are being considered for this equipment. The major change in the instrumentation was a result of replacing the micro-switch position sensors with optical switches. The commercially available optical switches consisted of a LED and a phototransistor built into a single unit. The advantage of this device was that it was much less sensitive to the mechanical adjustment of the switch-holding brackets. The probe position measuring system was also modified to provide a digital display to the pilot. This was necessary because the pilot could not see the probe for portions of its travel. Additional controls were added to the system to allow the pilot to operate the probe without diverting his attention excessively. The operation of the probe position system included a stepping control that allowed the pilot to step the probe vertically in one-inch intervals. The probe could also be operated vertically in a free-running mode, but this mode was not used during test runs. The horizontal position of the probe was given by recorded voltage steps that were initiated by the optical switch encountering position pins that were attached to the boom. The pins were located at one-inch intervals along the boom. The signal from the optical switch activated a relay which put the output from the anemometer thermocouple onto the number-seven data channel for a 100 mili second time period. A DC voltage bias was provided to insure that a well-defined voltage

step was obtained at each pin location. These recorded voltage steps were used as triggers for activating the A-D converter during the data reduction process.

The instrumentation system was also modified to allow the probe output information to be monitored and to improve the voltage calibration capabilities of the system. The trolley drive system was revised to eliminate certain mechanical deficiencies that were noted in the previous program.

The instrumentation support equipment carried on the test aircraft was essentially the same as was used in the previous program. It included an inverter, batteries for the tape recorder and the probe position control system, signal conditioning equipment and a digital voltmeter.

Section III

Test Technique, Data Reduction and Accuracy Estimation

1. Test Technique

The operation of the test aircraft and instrumentation was conducted so as to duplicate the test conditions of the previous test program as closely as possible. The test flights were conducted soon after sunrise and only under calm atmospheric conditions. The tests were conducted between pressure altitudes of 4000 and 6000 feet with the ambient temperature at these altitudes varying between 32 and 53 degrees Fahrenheit. Aircraft power settings during the test runs provided straight and level flight at a propeller speed of 2400 revolutions per minute. The test runs were flown with the ball of the turn-and-bank indicator centered and the aircraft wings level.

Preflight checks were made on the test instrumentation prior to each test flight. These checks included cleaning the probe, verifying the factory calibration of the anemometer, servicing the data recorder and checking the calibration of the digital voltmeter. In addition to the preflight checks, voltage calibration data were recorded at test altitude - before and after the test runs for each flight. The calibration values were measured with the digital voltmeter.

2. Data Reduction

The instrument error and the static-pressure-source position error corrections were applied to all of the aircraft data. No compressibility corrections were used. The calculation of the aircraft trimmed lift coefficient, used in nondimensionalizing the vorticity data, was based on a mean test weight of 2520 pounds. A value of 0.0023769 slugs per cubic foot was used for the standard sea level density. The atmospheric model used in data reduction conformed to the U. S. Standard Atmosphere, 1962. The calibration equations and constants used for the anemometer data were supplied by the probe manufacturer.

The data processing procedure was considerably improved over the procedure that was used in the previous program. These improvements were made possible by the addition of a magnetic tape deck to the A-D converter/minicomputer that was used to process the test data. With the present system the analog test data were translated to digital form, through the A/D converter, and stored on the digital magnetic tape under the control of the minicomputer. The digital data were then converted to a format that was compatible with the UNIVAC 1106 computer through suitable programming. The utilization of the anemometer calibration equations along with the computation of the vorticity components and the subsequent machine plotting of the resulting data were then accomplished on the 1106 computer and the related peripheral equipment.

The voltage calibration of the complete instrumentation system was accomplished by assuming a linear relationship between the known input calibration voltages, recorded in flight, and the final values of the corresponding translated calibration data. Calibration constants were obtained for each data channel and each test flight. These calibration "constants" were used to convert the translated data to the correct voltages. The anemometer calibration equations were then applied to the voltage data. The translated calibration data represented the average 197 samples of the recorded analog data. The test data were the average of ten samples of the analog data taken at each position-pin trigger. Because of the limited size of the minicomputer, the raw voltage data was averaged rather than the final velocity data.

The ambient temperature data obtained from the anemometer unit was not used in reducing the velocity data because of excessive noise that was present on the analog recorder channel that was used to record the temperature data. The noise level did not prevent the position trigger information from being used, but it was of sufficient magnitude to make much of the temperature data useless. The temperature data recorded by the pilot, using the aircraft outside-air-temperature gauge, was used for the data reduction. The ambient temperature and the static pressure were used in the anemometer calibration equations and in obtaining the aircraft true airspeed.

The derivatives of the measured velocities, required in defining the components of vorticity, were computed using a 3-point collocation-polynomial finite-difference representation of the derivation. A central difference scheme was used for all of the x derivatives and for the y and z derivatives inside the measurement plane border. Backward or forward difference schemes were used in the border region. The vorticity data that are identified as representing the forward measurement plane (as opposed to the data shown specifically for x = 5.1 and 9.1 inches) are based on the y and z derivatives of the velocity components that are the average of the data obtained in the two forward measurement planes. The sign convention used in computing the components of vorticity is based on the longitudinal component (ζ_x) being positive aft, the lateral component (ζ_y) being positive outboard and the vertical component (ζ_z) being positive upwards. The vorticity data are normalized with respect to the product $U_t C_{L_T}$.

The angle between the resultant velocity vector and the resultant vorticity vector was obtained through the vector dot-product relationship

$$\theta = \cos^{-1}\left[\frac{u\zeta_x + v\zeta_y + w\zeta_z}{|\bar{U}|\,|\bar{\xi}|}\right] 57.2964$$

3. Estimated Accuracy

It is estimated that the aircraft indicated airspeed was maintained within ±0.5 miles per hour for at least 95 percent of the test data. Data acquisition was not attempted if speed excursions of 1.0 mile per hour were being experienced. Considering all sources of error for the airspeed determination, it is estimated that the equivalent airspeed is known within ±1.0 miles per hour. The aircraft weight was always within 1.5 percent of the mean test weight (2520 pounds) and within 0.5 inch of the mean center of gravity (40.0 inches).

The advertised accuracy of the total-vector anemometer is given as ±3 percent of the magnitude of the velocity vector and ±3 degrees of the velocity vector angle. Based on checks made in the previous test program, the accuracy of the final velocity measurements is considered to be within ±5 percent and ±5 degrees. This accuracy includes the operation of the complete instrumentation and data reduction systems.

In Reference 1 an evaluation of the accuracy of the vorticity calculations was made based on an estimate of the positional accuracy of the probe positioning system and the accuracy of the velocity measurements. Experience gained in measuring the position of the boom support structure during the present program has given cause to reconsider the earlier estimate. Measurements made before and after certain of the test flights have shown changes in the boom position, relative to the aircraft, of as much as 0.2 inch. Most changes were less than this amount, but they were greater than the 0.05 inch given in the referenced report. Changes of 0.05 inch were found, at times, as the aircraft structure temperature changed due to varying amounts of sunlight passing through the hangar windows. Based on these revised estimates, the final vorticity values are now considered to be accurate within ±10 percent.

Section IV

Test Results

1. General Discussion

The results of the present test program are presented and discussed in the following paragraphs. Most of these data are presented as contours of constant values of the components of vorticity. Velocity component data are not presented because they do not add new information to that already shown in Reference 1. New wing span-loading data were not obtained in the present test program because the span-loading data shown in reference 1 are still considered to be valid for the present test results.

For the most part, the data obtained in the present test program exhibit the same basic characteristics of the earlier test data. The consistency of the new data, when compared to the results obtained two years previously, is considered to provide impressive verification of the ability of the equipment and the test technique to yield accurate wake velocity data under actual flight conditions. Comparisons of the measured velocities in the upper mid-semispan portion of the measurement plane, where velocities should be near free stream, have shown that the data from both test programs are within the estimated five percent accuracy of the complete instrumentation system. There are certain differences between the two sets of test data, however, that cannot be satisfactorily explained at this time. These differences are beyond the bounds of the estimated accuracy of the computed vorticity (see Section III). These differences consist of a reduction in the peak values of vorticity and a moderate change in the distribution of the vorticity around the peak concentration of vorticity near the wing tip. These differences are consistent within the present test program and would seem to rule out non-steady flow considerations.

The peak values of vorticity found in the present test are ten to twenty percent lower than found earlier. The contours for the moderate values of vorticity, however, are essentially unchanged. Although it is difficult to characterize the change in the distribution of vorticity about the peak value of positive vorticity near the wing tip, it would appear that the distribution has rotated counterclockwise about the peak value by about 45 degrees. The consistency of the test results within each test program would seem to indicate that there is some undetected aircraft configuration change between the two test programs. The only configuration differences that can be suggested are a change in the BLC system performance and a change in the travel limits of the wing flaps. Failures were experienced during the initial phase of the present test program with both of the hydraulic motors that power the BLC system. These units were replaced and there was no noticable change in the

performance of the system. It is doubtful that minor reductions in BLC performance, considering the moderate lift coefficients being used, would produce the noted changes in vorticity. A failure also occurred in the flap drive gear box early in the present program. Replacing this unit required adjustment of the flap drive limit switches, but the observed flap travel was not changed by this adjustment. One additional potential source for the reduced magnitude of the vorticity is the determination of the value of the product $C_{L_t} U_t$ that is used to normalize the vorticity data. An excessive value of this product would yield the lower values of vorticity, but all known precausions were taken to insure correct values of the trimmed lift coefficient and the true airspeed. As far as can be determined, these suggested sources for the observed differences were adequately controlled in the test program and are not thought to have contributed to these differences. Although no satisfactory explanation can be given for the noted differences, it is felt that these differences do not significantly detract from the value of the results. These data do represent the most detailed and accurate presentation available on the distribution of vorticity in the near wake of a flight-test vehicle.

Some liberties have been taken with the presentation of the results of this test program in the interest of minimizing the complexity of the contour plots. Although an effort was made to present a consistent range of vorticity contours, some contours have not been shown when they are in very close proximity to the contour of the next higher value. With very few exceptions, leaders identifying the magnitude of the contours are provided. Only one leader is used for each contour, and it is sometimes necessary to trace the perimeter of the contour to find the leader. In those cases where it was not possible to use a leader on a contour, the values of the adjacent contours and the increments in the values being used will make the correct value of the contour in question obvious. Certain of the contours shown in this report are made with a broken curve to indicate that there is some question as to the validity of the contour. These questionable contours occur in the region where data from different test flights occupy adjacent rows in the measurement plane. It is suspected that these contours are a result of minor differences between data obtained on different flights rather than a real variation in the flow field.

The interpretation of the vorticity contours for the outboard half of the measurement plane is fairly straight forward and does not require explanation. The inboard half of the measurement plane, on the other hand, does require comment in order that the reader may properly interpret the figures. There are three dominant factors that determine the character of the wake seen in the inboard half of the measurement plane. The propeller slipstream is all that is seen within the first 30 or 40 inches of the measurement plane. Only representative contours are shown in this region because the propeller slipstream is not of interest in

the present program. The BLC blower wake dominates the measured data from 40 to 70 inches out on the measurement plane for the zero-flap configuration. The two blowers, one under each wing, pump a total of 8000 cubic feet per minute of air with exit velocities on the order of 120 feet per second. The blowers are axial flow fans with one final stage of straightening vanes. The flow field in this region represents the cimbined influence of the external flow over the blower fairings and the blower exhaust. The outboard end of the flap and the flap end plate are located 85 inches out on the measurement plane. It would appear that the end plate is responsible for the vertical array of vorticity that is found near the 80 inch position for all zero-flap data. The fact that the full-up position of the flap (zero flap deflection) does not eliminate all incremental flap loading also contributes to some of the vorticity concentration found in this area. The span loading data given in Reference 1 shows the slight change in the spanload gradient at the outboard end of the flap for the zero-flap configuration. For the full-flap configuration the region of the measurement plane from 60 to 100 inches is dominated by the vorticity generated by the outboard end of the flap.

A summary of the test conditions that were used in the present test program are given below:

Measurement Station	Flap Deflection	U_e (mph)	U_t (mph)	C_{L_t}	α (deg)
fwd (X = 5.1 in.)	zero	61.0	65.6	1.498	18.3
fwd (X = 5.1 in.)*	full	60.5	65.2	1.523	10.7
fwd (X = 9.1 in.)	zero	61.0	65.9	1.498	18.3
fwd (X = 9.1 in.)*	full	60.5	65.2	1.523	10.7
mid (X = 33.3 in.)	zero	60.7	64.4	1.513	18.4
mid (X = 33.3 in.)	zero	80.1	85.3	0.869	12.3
mid (X = 33.3 in.)	full	60.6	64.8	1.518	10.5
mid (X = 33.3 in.)*	full	79.1	84.9	0.888	5.1

The data for the test conditions shown with an asterisk could not be analyzed because of the aircraft and instrumentation problems. The instrumentation problems rendered the recorded data unsuitable for processing through the A-D converter, and the schedule slippage, resulting from the aircraft problems, did not allow the test flights to be repeated.

2. Angular Relationship Between Vorticity and Velocity

One of the objectives of this experimental program was to determine if there was any significant agreement between the directions of the vorticity vector and the velocity vector within the near wake. Aside from the theoretical implications that collateral behavior may have, it was felt that such behavior might allow the determination of all the components of vorticity with only a single velocity measurement plane rather than the two closely-spaced planes used in the present program. If the vorticity vector was known to be parallel to the velocity vector, all vorticity components could be obtained from knowing the direction of the velocity vector and the magnitude of one component of the vorticity vector. To evaluate the relative direction of the velocity and vorticity vectors, the angle between those vectors was computed throughout the mean forward measurement plane. The components of the velocity vectors were the average of the components of the velocity vectors measured in each of the two forward measurement planes. The contours of constant values of the angle between the velocity and vorticity vectors are presented in Figures 5 and 6. The data show that the angular differences are pronounced and would offer little chance to obtain valid vorticity components based on the direction of the velocity data. A significant factor in this angular difference can be related to the boundary - layer flow which leaves the wing trailing edge with a significant spanwise component of vorticity but a velocity that is mainly in the chordwise direction.

3. Components of Vorticity in the Mean Forward Measurement Plane

The contours of the three components of vorticity found for the zero-flap configuration at a mean distance of 7.1 inches aft of the wing trailing edge and a mean true airspeed of 65.7 miles per hour are shown in figures 7 through 12. The x component of vorticity is presented in figures 7 and 8. Except for the lower peak values and the altered distribution around the peak value at the wing tip, noted in the initial paragraphs of this section, these data are consistent with the results of Reference 1. The wing wake appears higher in the measurement plane for the present data, as compared to the data of Reference 1, because the measurement plane is located 12 inches lower with respect to the aircraft wing in the present test program.

The contours of constant values of the y component of vorticity for the zero-flap configuration are shown in Figures 9 and 10. In general, positive values of the vorticity component are found above the center of the wing wake, and negative values are found below the center of the wake. This can be directly related to the momentum loss associated with the boundary-layer development over the surface of the wing where the vertical gradient of the chordwise component of velocity is negative in the lower surface of the wing and positive on the upper surface. This velocity gradient term is dominant in the spanwise component of vorticity

for a major portion of the wing wake. It is interesting to note that this component of vorticity is the only well defined component for the inner half of the wing where span-load variations are relatively small.

The contours of the z component of vorticity for the zero-flap configuration are presented in Figures 11 and 12. The interpretation of these data is not particularly obvious, but it can be noted that the magnitude of the vertical component is somewhat less than the spanwise component. In general, however, all of the components of vorticity are of the same order of magnitude except for the wing-tip region. In the tip region the x component of vorticity clearly dominates the flow field. Based on these results it can be noted that there is a significant portion of the near-wake vorticity that is not seen if the vorticity measuring system evaluates only one component of vorticity. This may be a factor in the failure of past near-wake measuring projects to account for all of the vorticity that is predicted based on span-load data. For the data previously obtained on the test aircraft used in the present program, Damania (see Reference 2) has found that the integration of the x component of vorticity yields about 65 percent of the vorticity predicted from the span-load data. Although time did not permit similar calculations using the resultant vorticity magnitude found in the present program, such results should yield values in close agreement with the span-load results. However, some additional study is required regarding the use of the resultant vorticity values, since the relationship between the spanwise component of vorticity and the span-load distribution may be questioned.

A comparison of the x components of vorticity obtained in the two forward measurement planes (x = 5.1 and 9.1 inches) for the zero-flap configuration and an average true airspeed of 65.7 miles per hour is shown in Figures 13 and 14. Only small differences are seen between the data obtained in the measurement planes which had only 4 inches of longitudinal separation. One can see the early stages of the diffusion of the vorticity component which is also accompanied by a tendency for the more uniform vortex sheet to form into a distribution of vortex tubes. Comparing these figures with Figures 7 and 8 shows the smoothing effect that results from the averaging of the velocity data. The wake is slightly higher in the measurement plane located 9.1 inches aft of the wing because the alignment of the measurement planes is inclined with respect to the free stream (i.e., the perpendicular to the measurement planes is at an angle of attack with respect to the free-stream velocity). This inclination results in the wake intersecting the measurement planes at higher values of z' as it moves aft from the wing in spite of the downwash that results from the wing lift.

4. Vorticity data for the Mid Measurement Plane

The contours of the constant values of the x component of vorticity for the zero-flap configuration, a true airspeed of 64.4 miles per hour and the measurement plane located 33.3 inches aft of the wing trailing

edge are shown in Figure 15 and 16. This location is approximately midway between the forward and the aft measurement planes of Reference 1. The aft measurement plane of Reference 1 was 61.2 inches aft of the wing trailing edge. Additional vorticity diffusion is shown by these data. A comparison of these figures with Figures 16 and 17 of Reference 1 shows that the trailing wake of the wing had not yet developed the curvature that is quite apparent in the aft measurement plane data of Reference 1.

The contours of constant values of the x component of vorticity in the mid measurement plane for the full-flap configuration at 64.8 miles-per-hour true airspeed are presented in Figures 17 and 18. It is unfortunate that the corresponding forward measurement plane data were not usable, but suitable comparisons can be made with the data of Reference 1. More details of the vorticity generated by the flapped portion of the wing are found in the present data. The lack of wake curvature at this mid plane as compared to the aft plane of Reference 1 is again illustrated.

The contours of the x component of vorticity in the mid measurement plane for the zero-flap configuration at a true airspeed of 85.3 miles per hour are shown in Figures 19 and 20. These data are consistent with the results of Reference 1. No explanation can be given for the vorticity found in the lower outboard portion of the measurement plane shown in Figure 20. These results would not show up in the Reference 1 results because of the higher placement of the measurement plane. This vorticity must be suspect, however, since no source for such a flow field can be envisioned.

Section V

Longitudinal Stability Analysis of Trailing-Wing Probe Support System

1. Background

For a proper understanding of the rolling-up process of the wing-wake, generated by an aircraft in flight, velocity and vorticity measurements are required at various measurement planes behind the wing of the test aircraft. Although wake measurements are desired over a significant range of distances behind the generating wing, the current interest is in the region where the initial phases of the roll-up process are taking place. The present research program is providing data within one chord length of the wing trailing edge. The goal of this analysis is to evaluate the feasibility of a device that will provide wake data four chord lengths behind the wing trailing edge (i.e., the measurement will be aft of the generating aircraft tail plane). Earlier investigations conducted at Mississippi State University using a towed glider as a chase aircraft were not very encouraging because of the problems associated with an accurate determination of the relative position of the glider behind the tow airplane. For these tests the tow airplane was also the vortex generating aircraft. Other investigators have reported difficulty in achieving an inherently stable tow configuration.[3] In the present case, however, the desired distance between the test aircraft and the measurement plane is of the order of 10 feet, and a rigid 'tow-bar' connecting the trailing wing to the airplane is found feasible. This tow-bar' is in the form of two parallel A-frames; an arrangement which maintains the incidence of the trailing wing with respect to the aircraft reference line a constant. A wing is arranged in such that it supports the weight of the complete boom-structure including the anemometer probe. Control of the trailing wing is achieved by providing a trailing edge flap on the wing. The analysis carried out herein shows satisfactory stability and indicates that the control characteristics should be adequate for the combination of the trailing wing and aircraft.

2. Description of the Trailing-Wing System

The purpose of the trailing-wing system is to provide a platform, aft of the aircraft, to support the boom structure used for wing-wake measurements. A scale drawing of the proposed trailing-wing system is provided in Figure 21. The chief feature of this device is the parallel A-frame arrangement which links the aircraft and the trailing wing. The action of the parallel A-frames is to maintain the incidence of the trailing wing with respect to the aircraft. This arrangement overcomes the apparent lack of stability found with towed gliders which have relative freedom in pitch.[3]

A wing-tip drag wire is connected between the starboard wing tip of the aircraft and the outboard end of the boom. This drag wire supports part of the trailing wing drag load and inhibits vibration of the boom.

The trailing wing will be provided with ground adjustable incidence and a controllable flap. The flap will be divided into two elements with one providing a manual trim capability and the other used with the automatic control system. Dividing the control surface will allow adequate control power for large changes in flight speed and aircraft flap deflections while providing lower control sensitivity for the automatic control system. The anticipated control system will utilize a low-power laser beam and an array of sensors as the position measuring device. The laser unit will be mounted to the aircraft with the beam identifying the desired boom position relative to the aircraft. Sensors located on the boom assembly will identify the boom position relative to the laser beam and the appropriate flap deflection will be generated.

The center-line of the trailing wing is offset to the starboard side of the airplane longitudinal axis to help compensate for the eccentric loading imposed on it by the trailing boom.

The problem of interference between the A-frames and the aircraft control surfaces has been considered in configuring the support structure. The present design allows full elevator travel with -19 and +11 degrees of A-frame deflection. This corresponds to -43 inches and +25 inches of boom travel respectively. In the horizontal plane, the dimensions of the A-frame are quite adequate to accomodate maximum rudder deflection.

Operating an aircraft with a trailing-wing system such as described above does pose a number of control problems that must be considered. Operational techniques for landing and take-off will have to be evaluated and extensive testing of the device will have to be accomplished. Initial flight testing without the complete boom structure will be important. Finally, a device to jettison the entire trailing-wing system in an emergency seems to be desirable. The design of a suitable jettison device is not included in this analysis.

The structural analysis performed on the trailing-wing system was only intended to provide a realistic weight estimate of the system for use in the stability analysis. To this end, only the A-frame loading was considered, and the flight conditions consisted of straight-and-level flight, turning flight and a slipping maneuver. The critical stresses were found with the bending loads produced in the long A-frame members in turning flight. The turning maneuver consisted of a coordinated 2.5 g turn with the probe trolley positioned half way along the boom. No load relief due to the drag wire was assumed, and the bending loads were considered to be equally distributed between the 4 A-frame members. The slip maneuver assumed 15 degrees of slip, and that the bending loads were distributed equally between the A-frame members. A

1.5 safety margin was used in sizing the structural members. The maximum airspeed for this system was defined to be 90 miles per hour. The weight of the boom structure was based on the structure used in the present test program.

From experience gained at the Aerospace Engineering Department of the Mississippi State University in the construction of glider wings, the wing weight was estimated to be 1 pound per square foot of wing area. The resulting characteristics of the trailing wing system, as used in the stability analysis, are given below:

TRAILING WING DATA

Airfoil	:	65_3-618
Flap	:	20% Chord Ratio Sealed Flap
Wing Span	:	10 Ft
Wing Chord (Constant)	:	2.5 Ft
Wing Area	:	25 Sq Ft
Wing Weight	:	25 Lbs
Total Weight of the Trailing System	:	120 Lbs
Drag Coefficient of the Trailing Wing System	:	.1931 Based on Trailing Wing Area
Wing Lift-Curve Slope	:	4.9255 (Per Rad)

3. The Equations of Motion

The equations of motion are developed by application of Newton's laws to each of the aircraft's symmetric degrees of freedom. The trailing wing system is assumed to have a single degree of freedom with respect to the aircraft axes. The characteristics of the aircraft's modes of motion, including the trailing-wing system, are obtained by consideration of the roots of the resulting system of differential equations. The equations are non-dimensional form

$$2C_{\ell}\, u_1 + \{C_{\ell_\alpha} + h_1\lambda + C_{\ell_{\dot{\alpha}}}\lambda\}\alpha_1 + \{C_{\ell_{\dot{\theta}}}\lambda + h_2\lambda^2 - h_1\lambda + \ell_1\lambda^2\}\theta_1$$

$$+ \{C_{\ell_\delta} + C_{\ell_{\dot{\delta}}}\lambda + h_2\lambda^2\}\delta_1 = 0 \qquad (1)$$

$$\{C_{M_\alpha} + C_{M_{\dot{\alpha}}}\lambda\}\alpha_1 + \{C_{M_{\dot{\theta}}}\lambda - h\lambda^2\}\theta_1 + \{C_{M_\delta}\}\delta_1 = 0 \qquad (2)$$

$$\{C_L\}u_1 + \{\frac{C_{L_\alpha}}{2} + \lambda\}\alpha_1 - \{\lambda\}\theta_1 - \{\frac{C_d \cdot S_t}{2S}\}\delta_1 = 0 \qquad (3)$$

$$\{C_D + \lambda + C_d \frac{S_t}{S}\}u_1 + \{\frac{C_{d_\alpha}}{2} - \frac{C_L}{2} - \frac{C_R S_t}{2S}\}\alpha_1$$

$$+ \{\frac{C_L}{2} + \frac{C_R S_t}{2S}\}\theta_1 = 0 \ . \qquad (4)$$

where, u_1, α_1, θ_1 and δ_1 are the independent variables. Equation (1) is the equation of motion for the trailing wing with respect to the aircraft and Equations (2), (3) and (4) provide the equations of motion for the three symmetric degrees of freedom of the aircraft-boom combination. The following assumptions are made in the formulation of the equations of motion:[4]

(1.) In analysing the longitudinal stability of the aircraft, it is assumed that the disturbed motion is one of small oscillations about some steady-state flight condition and that the changes in external moments acting on the aircraft (due to this small departure from the steady state motion) depend on the displacement and disturbance velocities along and about the aircraft axes.

(2.) The major variables considered are the change in forward speed (ΔV), the change in angle of attack of the aircraft ($\Delta\alpha$), the change in the attitude angle of the aircraft ($\Delta\theta$), and the change in the deflection of the A-frame with respect to the aircraft ($\Delta\delta$). The aerodynamic forces and moments are evaluated in terms of first order approximations with respect to the independent variables and their time derivatives.

(3.) The motion of the trailing wing system is a rotation about an imaginary hinge line Y"Y" assumed to lie midway between the two sets of fuselage attachment fittings.

(4.) The drag coefficient of (C_d) the trailing wing system is assumed invariant with either the angle of attack of the trailing wing (α_t) or the deflection of the A-frames (δ). This assumption is based on the fact that a significant portion of the drag is associated with the support structure rather than the lifting surface.

(5.) Changes in the vertical forces on the aircraft due to the deflection of the A-frames are assumed to be negligible in comparison with the moments about the aircraft C.G. introduced by this deflection.

(6.) The trailing wing system is assumed to be in a uniform downwash field.

4. Stability Derivatives Due to the Trailing Wing

The derivation of the stability derivatives of the trailing-wing system and the changes in the aircraft stability derivatives due to the presence of the trailing-wing system is based on the following representation of the system.

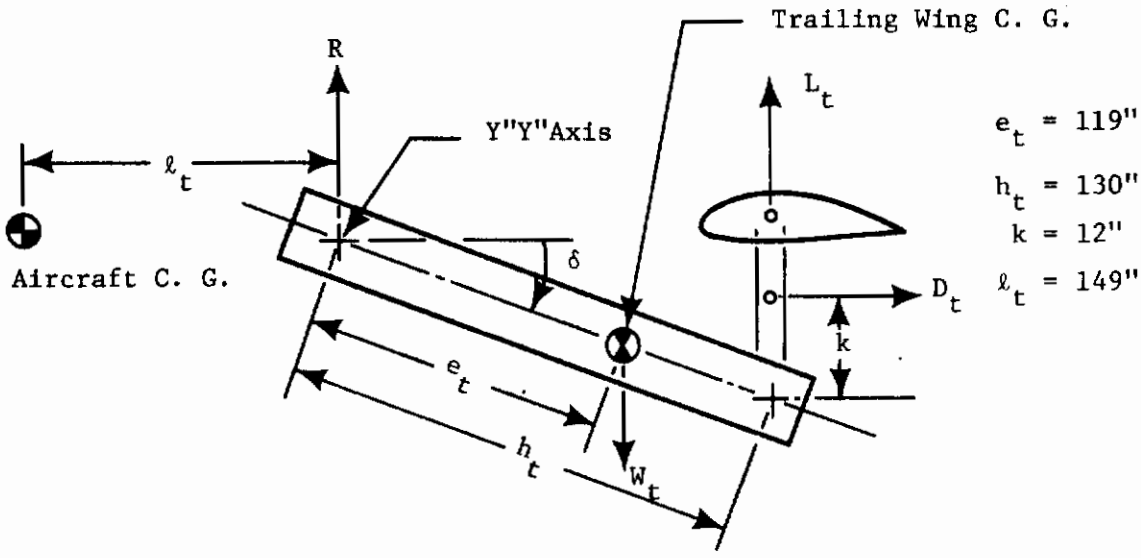

The reaction at the attachment point of the trailing-wing system to the aircraft (R) is defined as

$$R = W_t - L_t$$

It should be remembered that this reaction force is only considered in terms of the moment it develops about the aircraft center of gravity. It is considered to provide a negligible contribution to the vertical balance of forces acting on the aircraft. Taking moments about the Y"Y" axis for a steady position of the system

$$L_t h_t \cos\delta - W_t e_t \cos\delta - D_t(k - h_t \sin\delta) = 0$$

$$L_t = W_t \frac{e_t}{h_t} + D_t \left(\frac{k}{h_t \cos\delta} - \tan\delta\right)$$

and using the small angle approximation for δ

$$L_t = \frac{W_t e_t}{h_t} + D_t\left(\frac{k}{h_t} - \delta\right)$$

$$R = W_t\left(1 - \frac{e_t}{h_t}\right) - D_t\left(\frac{k}{h_t} - \delta\right)$$

$$C_R = \frac{W_t}{\frac{1}{2}\rho V^2 S_t}\left(1 - \frac{e_t}{h_t}\right) - C_d\left(\frac{k}{h_t} - \delta\right)$$

Considering the resulting moment about the aircraft C.G.

$$C_m = - C_R \frac{\ell_t}{C} \frac{S_t}{S}$$

$$C_m = \frac{W_t}{\frac{1}{2}\rho V^2 S} \frac{\ell_t}{C} \left(\frac{e_t}{h_t} - 1\right) + C_d \frac{S_t}{S} \frac{\ell_t}{C} \left(\frac{k}{h_t} - \delta\right)$$

Utilizing these relationships and considering the design flight condition of an equivalent airspeed of 90 miles per hour, the values shown in Table 1 were obtained.

5. Stability Characteristics of the Basic L-19

The characteristic modes of the stick-fixed longitudinal motion for most conventional airplanes are two oscillations; one oscillation is of long period with low damping and the other is of short period with heavy damping. For an aircraft with a time characteristic ($\tau = \frac{m}{\rho SV}$) of 1.5, typical aircraft yield a long period of approximately 32 seconds with a time to damp to half amplitude of 52 seconds and a short period of approximately 4 seconds with a time to damp to half amplitude of 0.5 seconds (see Reference 4). The L-19 test aircraft, without the trailing wing system, has a time characteristic of 1.37 and computed long and short periods of 21.9 and 2.2 seconds with the corresponding times to damp to half amplitude of 38.9 and 0.2 seconds. These computed values are in reasonable agreement with typical values for this type of aircraft and are considered to verify the estimated aerodynamic characteristics of the basic L-19. Further corroboration of the computed values was obtained from "hand" measurements of the long period motion of the basic L-19 in flight. The measured period was 26 seconds with the time to damp to half amplitude of 31.2 seconds. The short period characteristic of the test aircraft could not be measured but was heavily damped.

6. Discussion of Results

In order to study the characteristic motion of any dynamic system it is not necessary to determine the values of the variables concerned as functions of time. The thing that is important is to determine the character of motion - if oscillatory the period and damping, if aperiodic the rate of convergence or divergence. These characteristics for the airplane trailing wing combination as well as for the basic airplane

alone are tabulated in Table No. 2. The presence of the trailing wing does not significantly alter the short period characteristics of the basic airplane. In the case of the long period mode (phugoid), the period does not vary much and its damping is improved by the presence of the trailing wing. This is quite in accordance with the theory that increasing the parasite drag of the airplane will improve the damping of the long period mode and have small effect on the period. The trailing wing also introduces another short period mode (short period 1) with a period of the order of 10 seconds and the time to damp to half amplitude of the order of 1 second.

Table No. 3 shows the variation of the characteristics of these 3 modes of motion with a series of systematic changes of the trailing wing. It is once again seen that the short period characteristics of the airplane (short period 2) are not affected by the modifications to the trailing wing system. Wide variations in the weight of the trailing wing system, the trailing wing area and the drag coefficient of the trailing wing system similarly do not significantly alter the phugoid characteristics. For reductions in trailing-wing loading and drag-coefficient from the estimated values, the third mode (short 2) showed very large increases in the period and only slight changes in the damping (i.e. in effect, the oscillatory mode becomes a non-oscillatory convergence).

The presence of the trailing wing system produces a large increase in the static stability of the airplane. The static stability criterion $\frac{\partial C_M}{\partial C_L}$ for the basic airplane was found to be -.1425. With the trailing wing installed, $\partial C_M / dC_\ell$ became -.3568. This increase in stability may make aircraft control difficult and will call for the use of greater control forces on the part of the pilot. The relatively long period (low frequency) oscillation of the trailing wing system should make the trailing-wing control system requirements reasonable. Adequate control power for the trailing-wing system does not seem to pose a problem.

In conclusion it may be stated that the proposed trailing wing system towed by an airplane does not show any adverse stability characteristics. It is controllable and the system seems to be feasible.

Section VI

Conclusions

1. The ability of the wake measurement equipment and test technique to provide consistent, repeatable and accurate wake data has been demonstrated by this test program. Those areas in which satisfactory repeatability were not shown are considered to be the result of undetected aircraft configuration changes rather than deficiencies of the measurement system.

2. Proper evaluation of the near wake vorticity does require sufficient test data to allow the determination of all components of vorticity. Attempts to assume that the vorticity and velocity are collateral will not be satisfacotry in the near wake.

3. Noticeable curvature of the wing wake does not develop within one-half chord lengths (0.15 b/2) of the wing trailing edge. An apparent diffusion of vorticity does show within this distance. (Based on an earlier test program, noticeable curvature of the wake is seen one chord length behind the wing.)

4. The analysis of the proposed trailing-wing system indicates that the concept is feasible. A detailed design of the system will require a more complete study of the control system and must make provisions for emergency release, and recovery, of the system. It is felt that this system can provide wake measurement data at distances of the order of four-chord lengths (greater than one semispan) behind the wing trailing edge. Measurement accuracy will be less than found in the present test program, but it will be much better than any alternate system that is currently being considered.

REFERENCES

1. Mertaugh, Lawrence J., and Damania, Rustom B., An Investigation of the Trailing Vorticity Behind a STOL Aircraft, AFFDL-TR-73-138, Mississippi State University, Mississippi State, Mississippi, December 1973.

2. Damania, Rustom B., Investigations of Near Field Wakes Behind High-Lift Wings, Ph.D. Dissertation, Mississippi State University, Mississippi State, Mississippi, December 1973.

3. Maryniak, Jerzy, "Longitudinal Stability of a Glider in Rigid Tow," Technical Soaring, Vol. II, 1, 1972.

4. Perkins, Courtland D., Hage, Robert E., Airplane Performance Stability and Control, John Wiley and Sons, Inc., 1949.

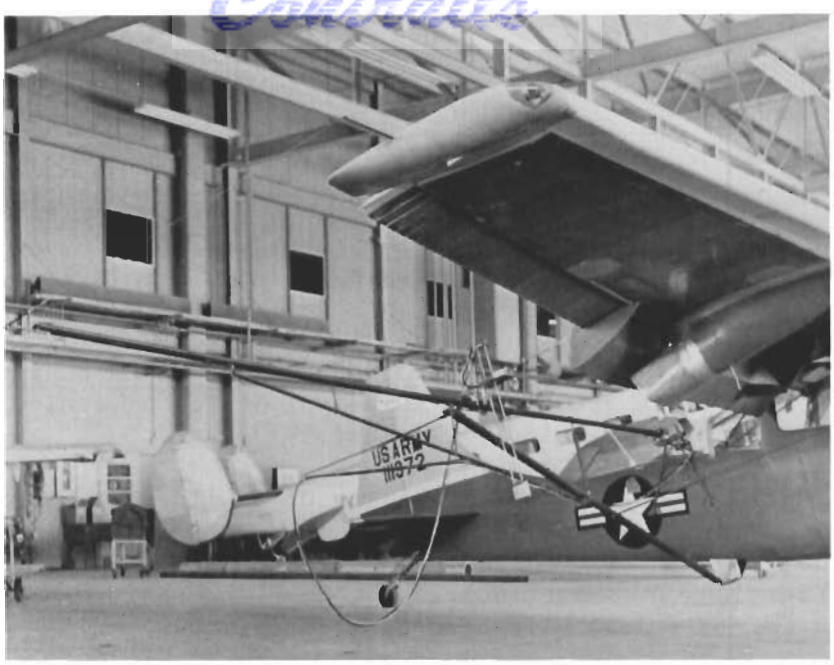

(A)

(B)

Figure 1. Test Aircraft with the Wake Measurement Boom in (A) the Forward Position and (B) the Mid Position

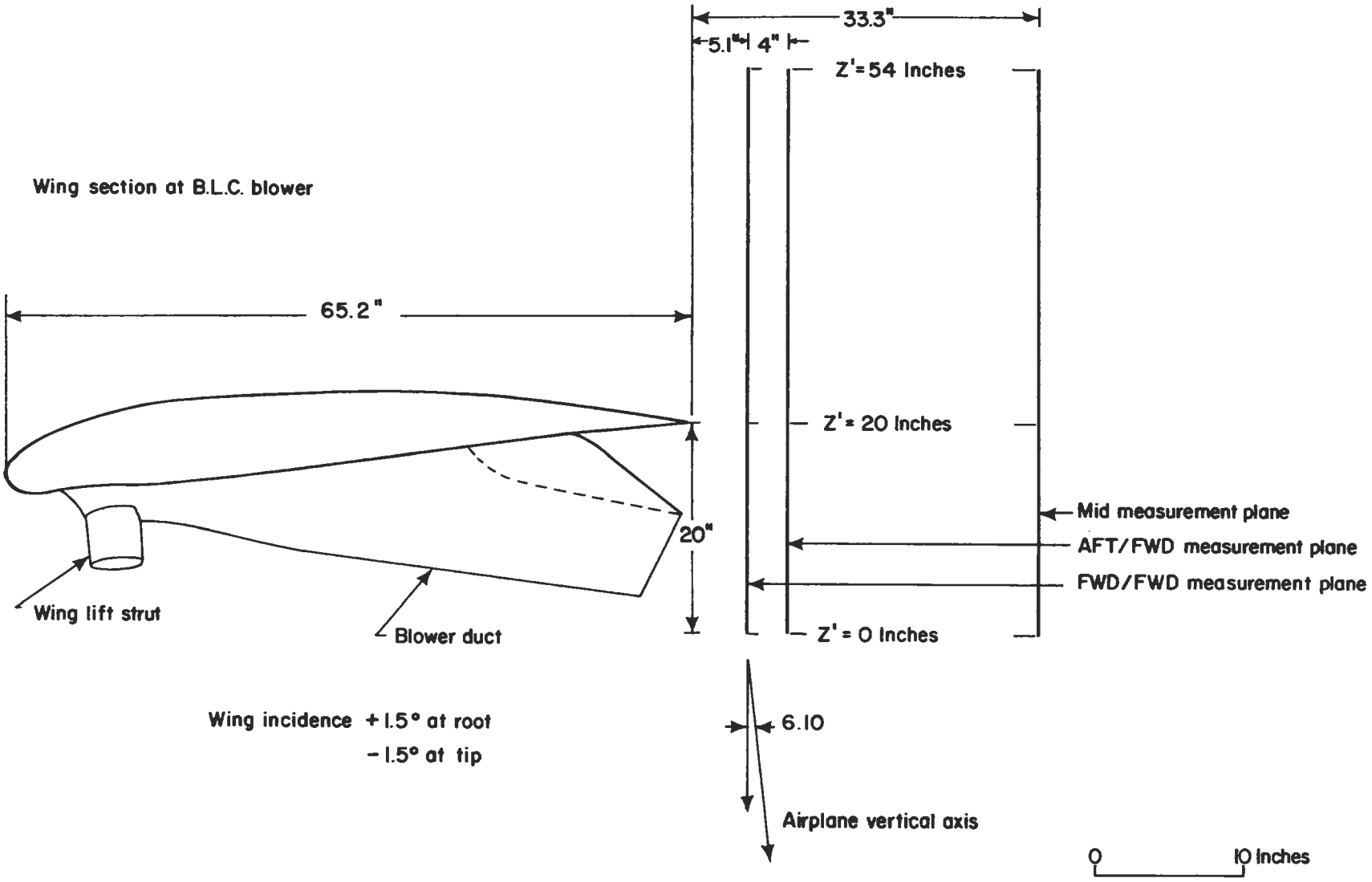

Figure 2. Side View of the Wake Measurement Stations with Respect to the Test Aircraft Wing

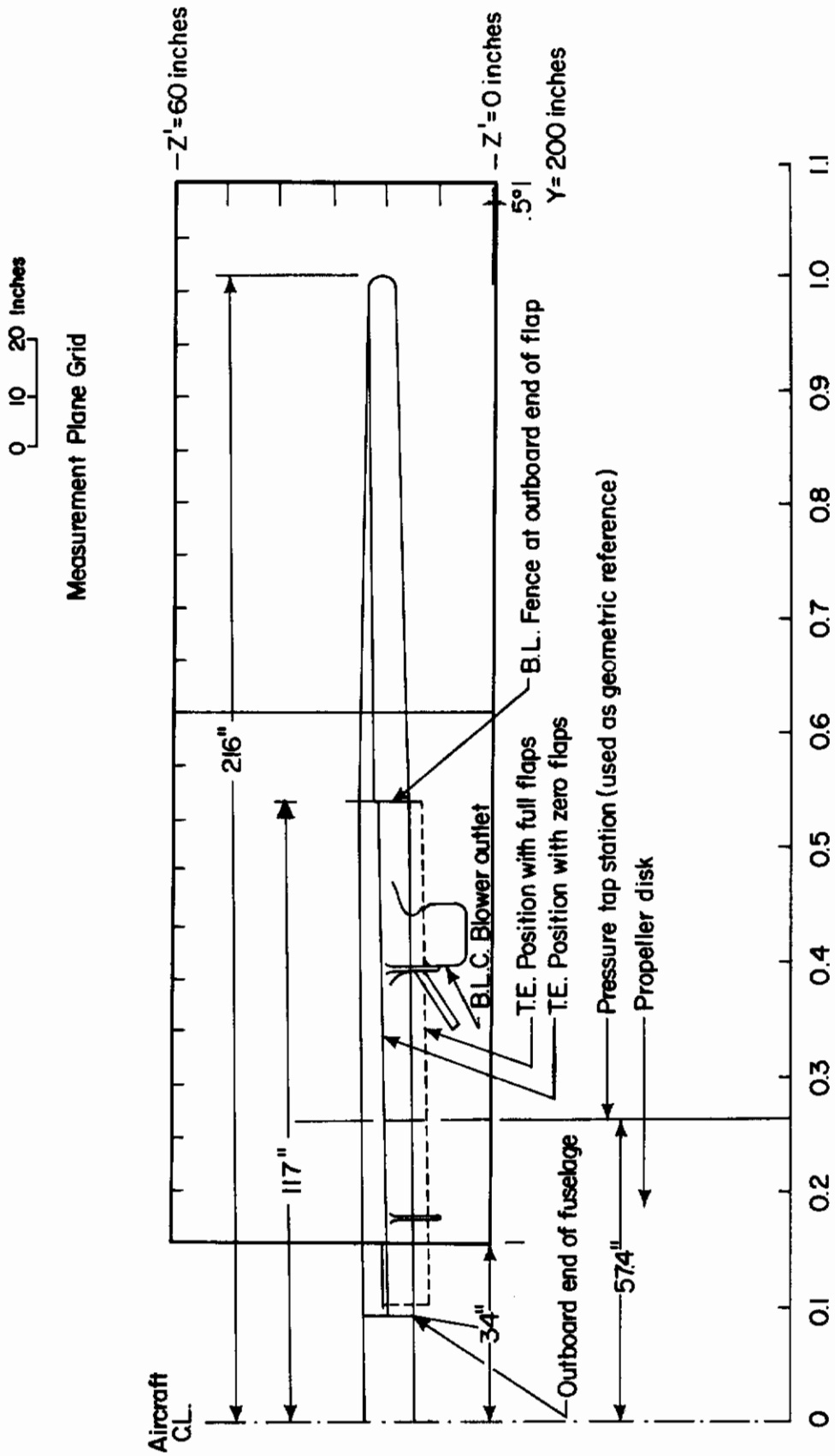

Figure 3. Forward View of the Wake Measurement Plane with Respect to the Test Aircraft Wing

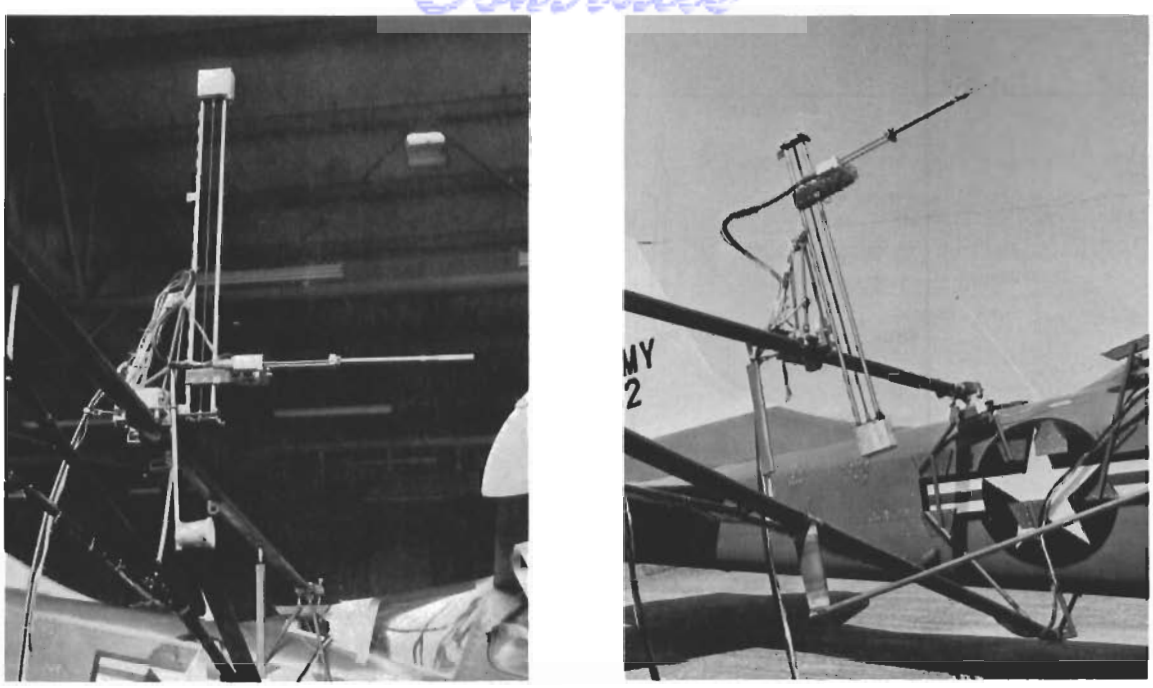

(A) (B)

(C)

Figure 4. Probe Vertical Traversing Mechanism in the (A) High Position, (B) Mid Position and (C) Low Position

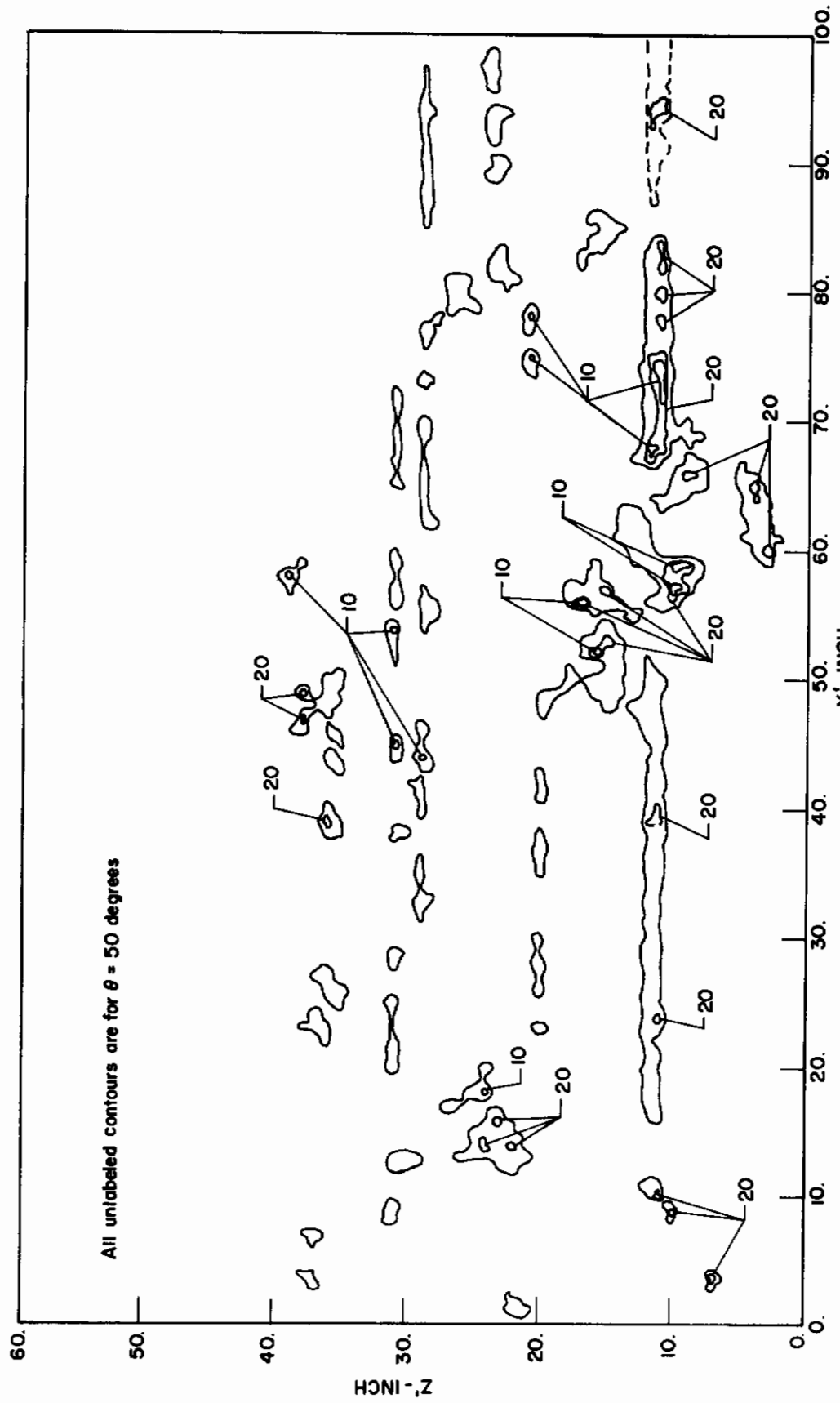

Figure 5. Contours of the Angle Between the Wake Vorticity and Velocity Vectors, Inboard Data, Zero-Flap Deflection, Forward Station, $\bar{U}_t$ = 65.7 mph

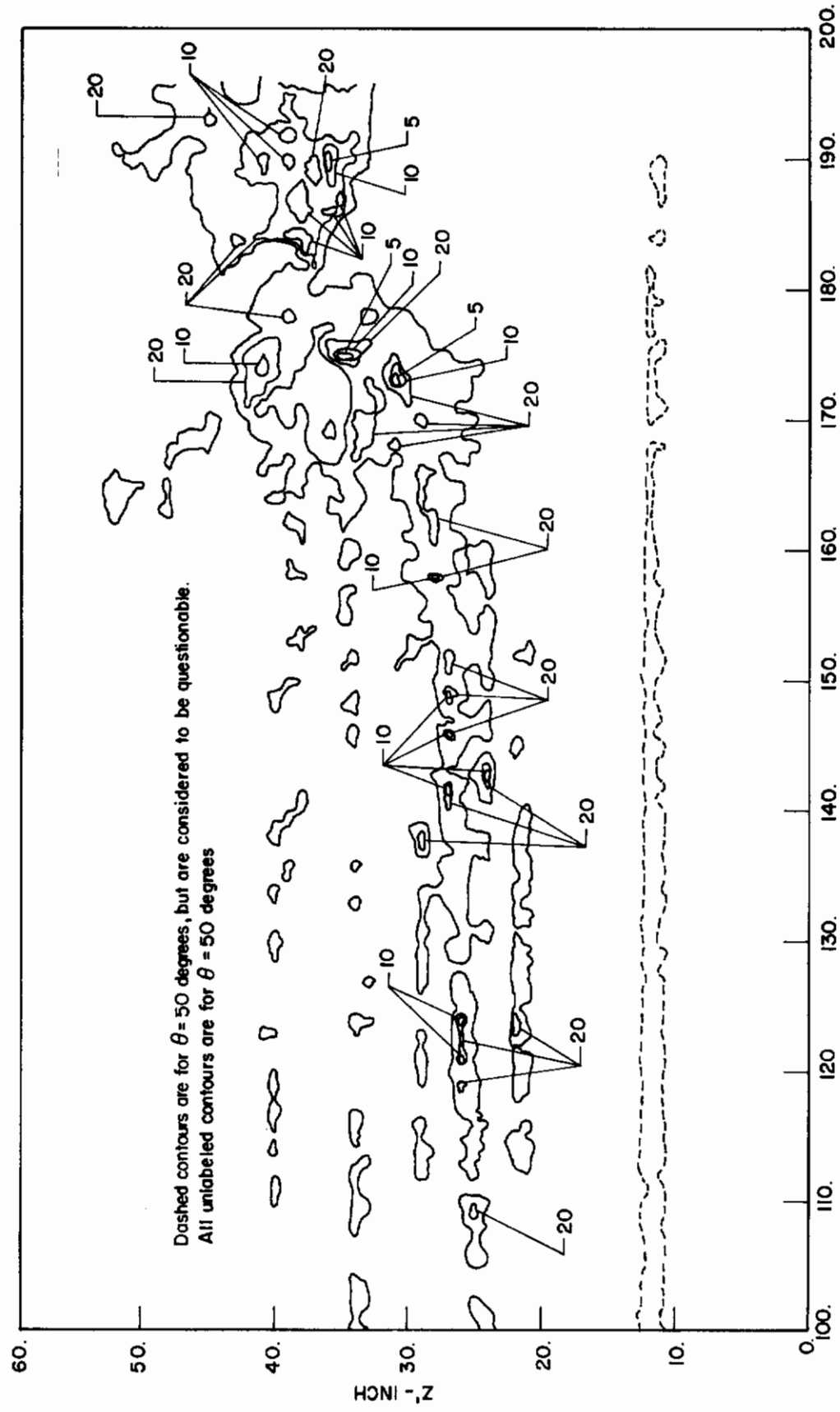

Figure 6. Contours of the Angle Between the Wake Vorticity and Velocity Vectors, Outboard Data, Zero-Flap Deflection, Forward Station, $\bar{U}_t$ = 65.7 mph

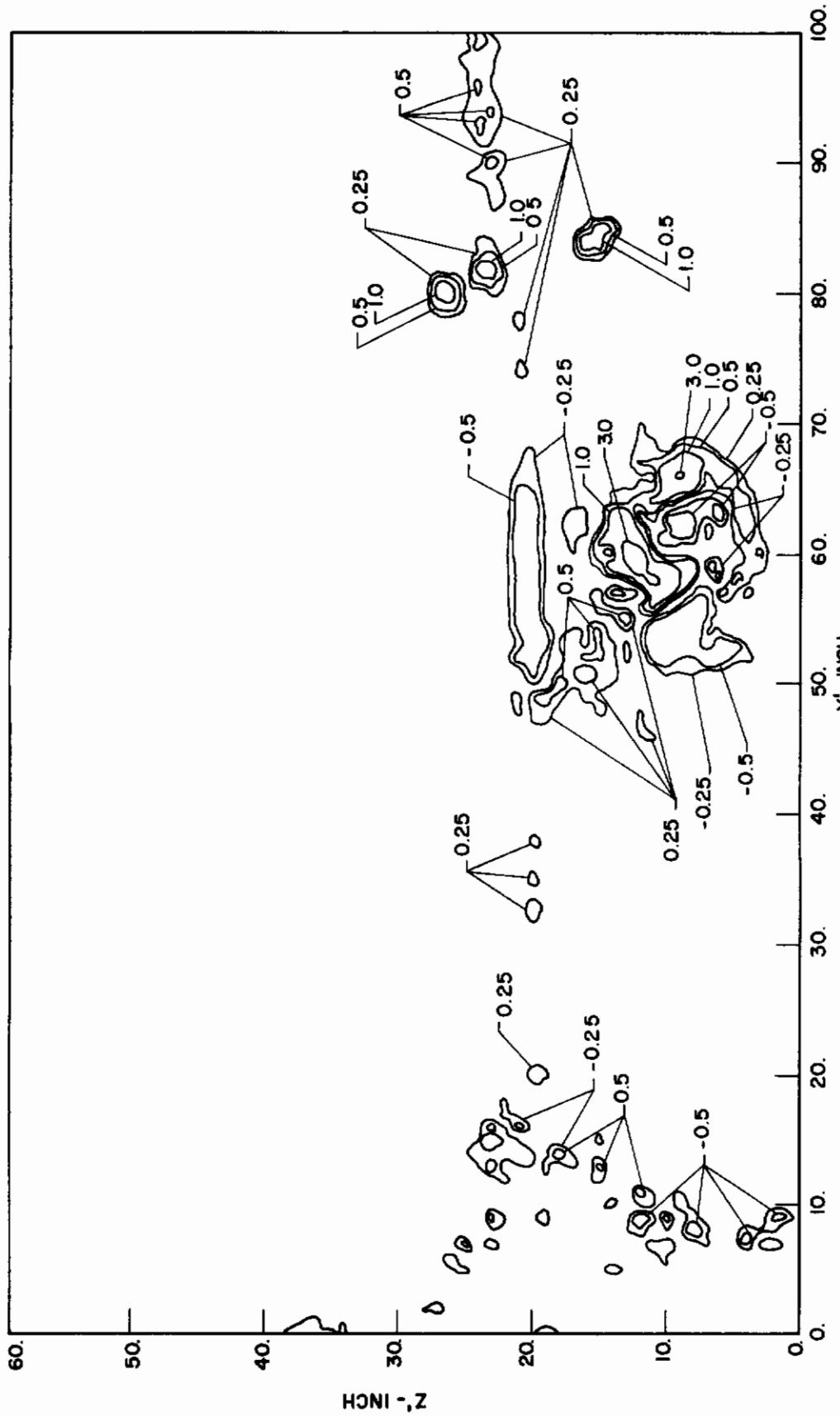

Figure 7. Normalized X-Component of Vorticity Contours, Inboard Data, Zero-Flap Deflection, Forward Station, $\bar{U}_t$ = 65.7 mph

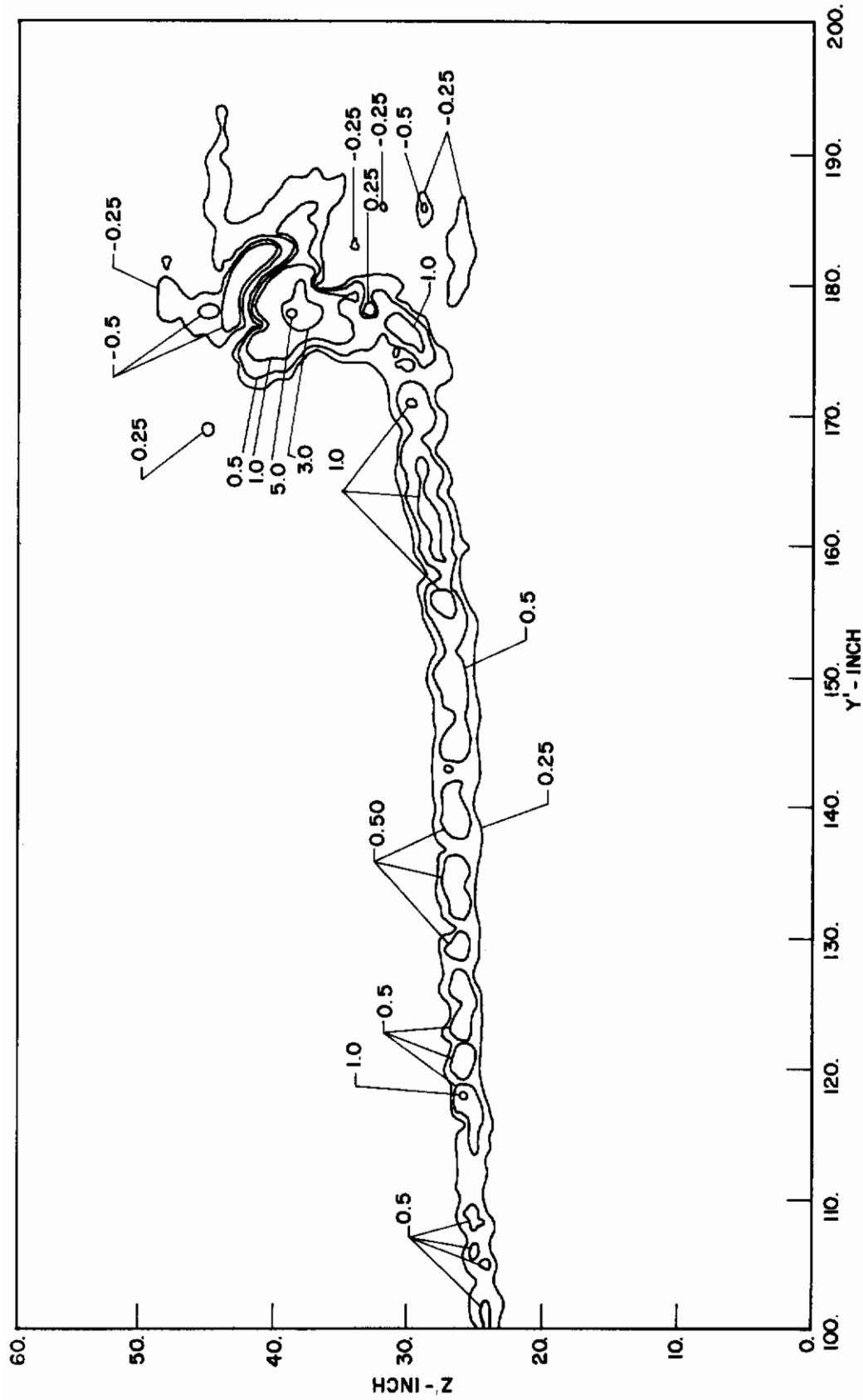

Figure 8. Normalized X-Component of Vorticity Contours, Outboard Data, Zero-Flap Deflection, Forward Station, $\bar{U}_t$ = 65.7 mph

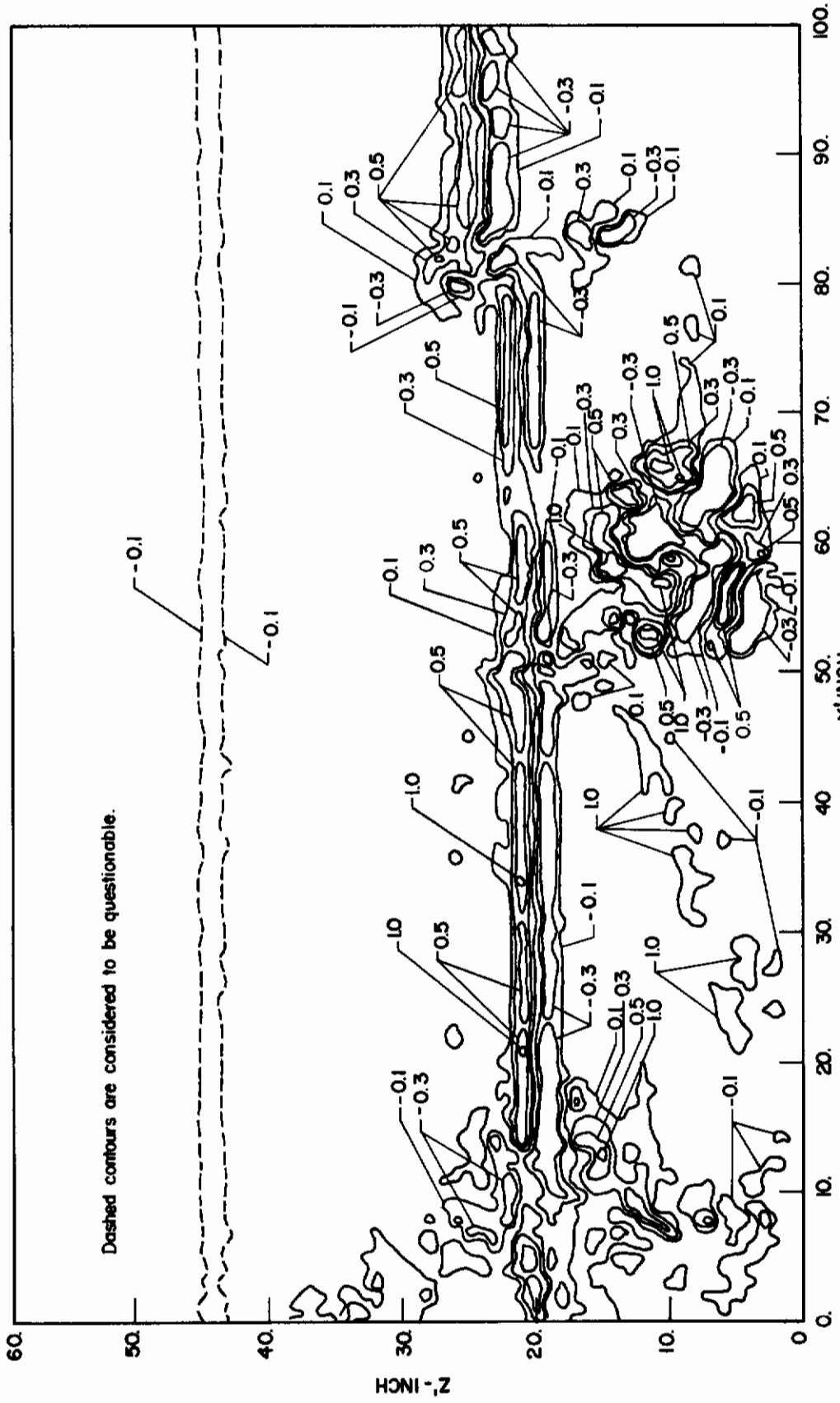

Figure 9. Normalized Y-Component of Vorticity Contours, Inboard Data, Zero-Flap Deflection, Forward Station, $\bar{U}_t$ = 65.7 mph

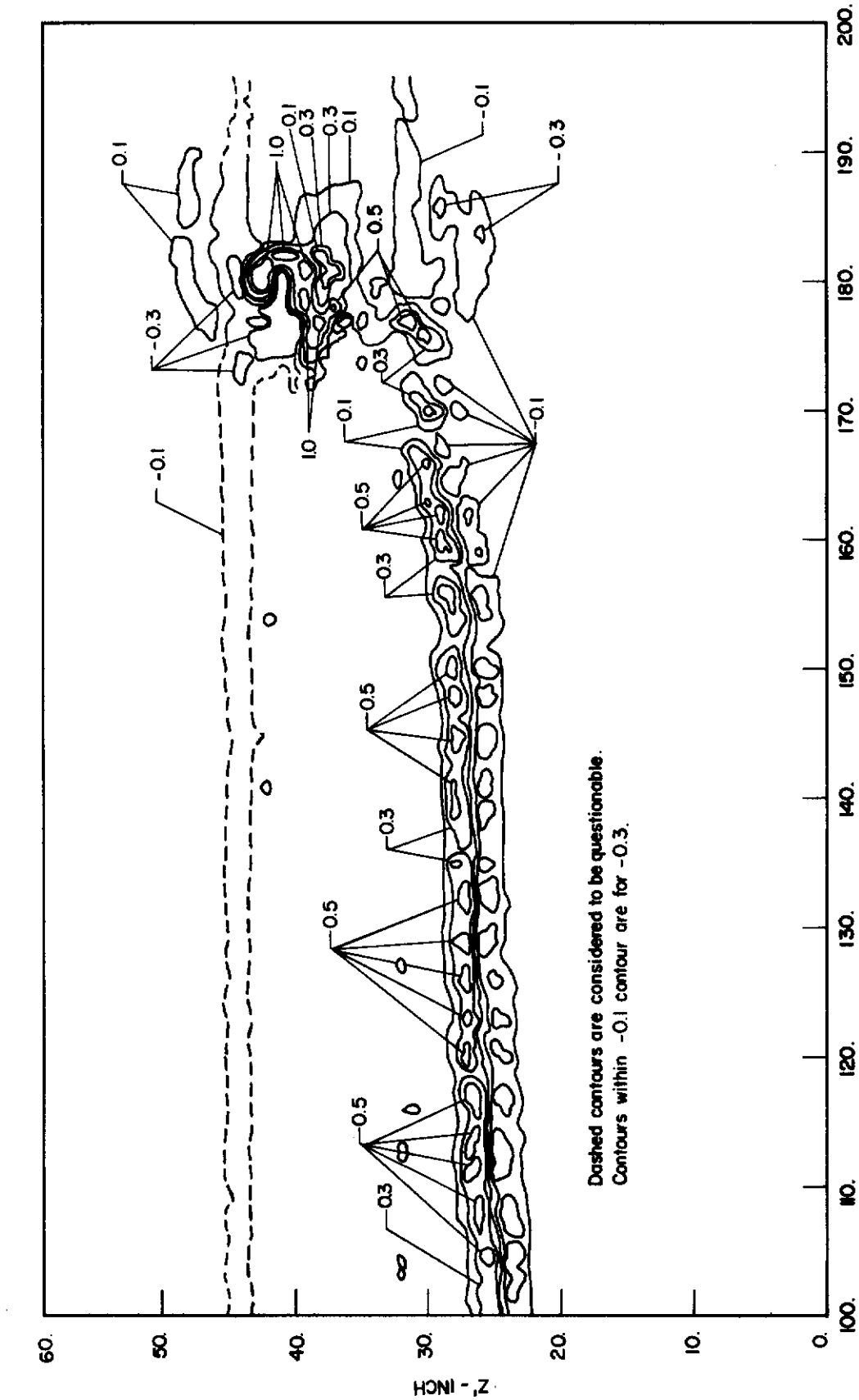

Figure 10. Normalized Y-Component of Vorticity Contours, Outboard Data, Zero-Flap Deflection, Forward Station, $\bar{U}_t$ = 65.7 mph

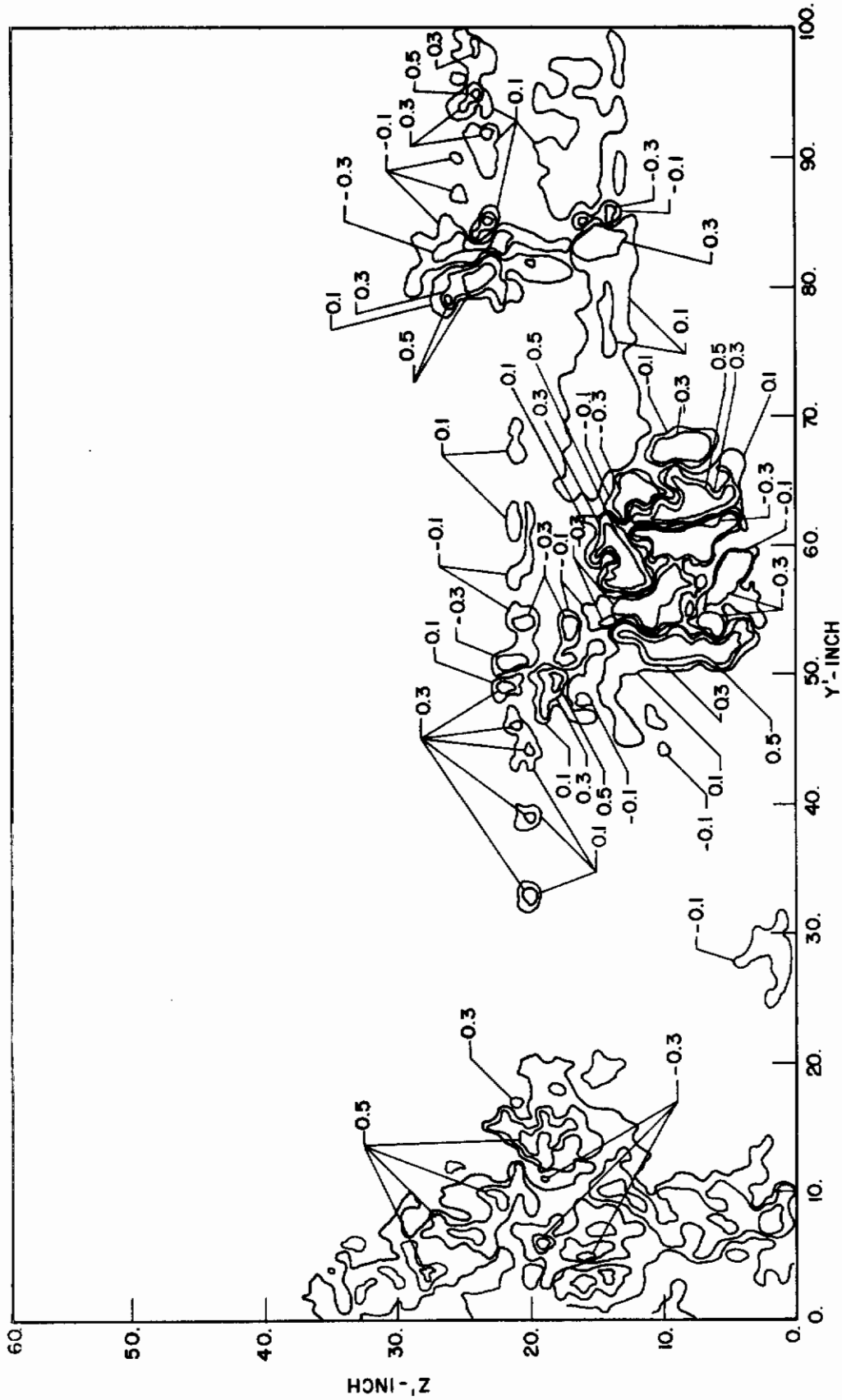

Figure 11. Normalized Z-Component of Vorticity Contours, Inboard Data, Zero-Flap Deflection, Forward Station, $\bar{U}_t$ = 65.7 mph

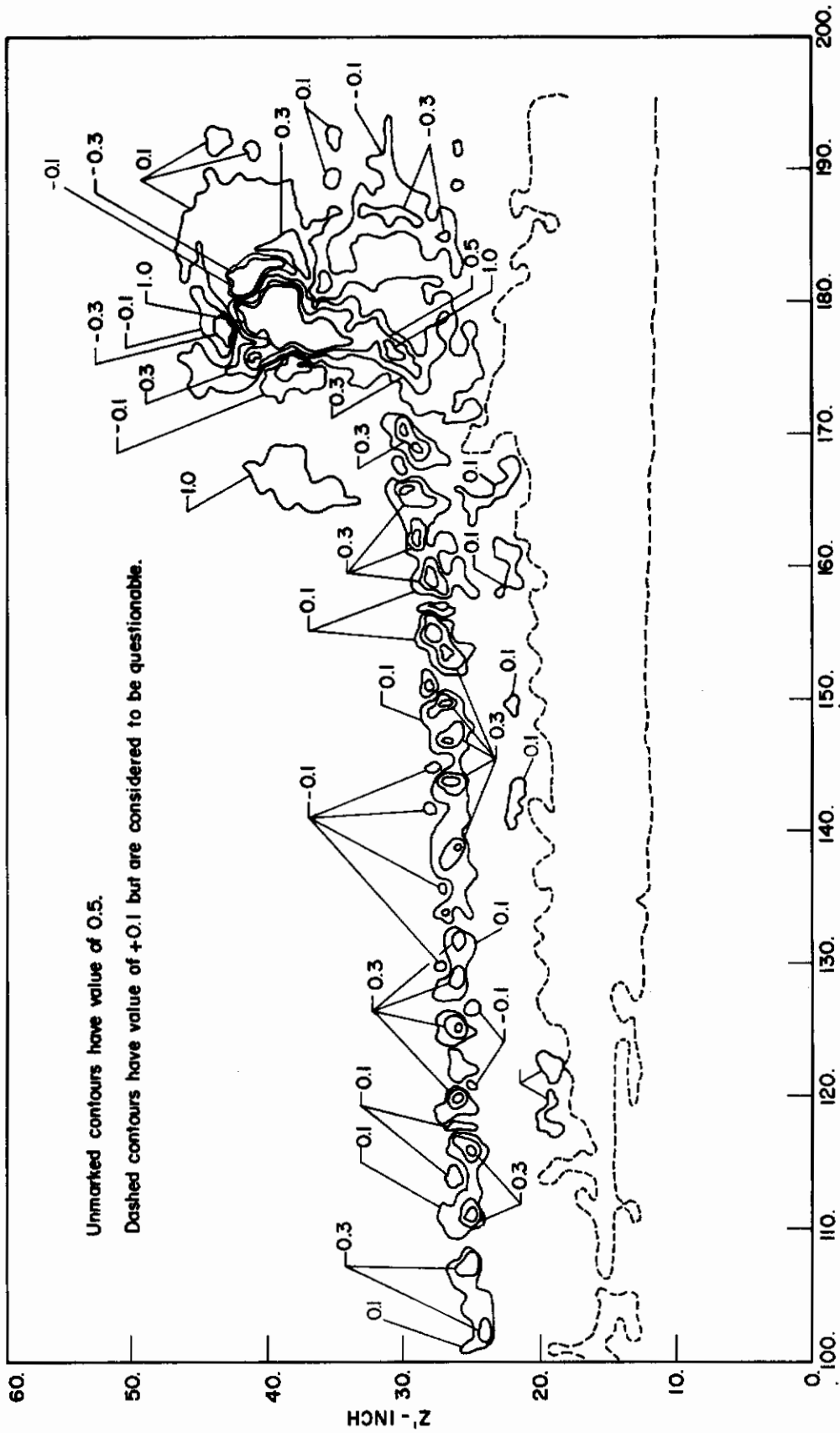

Figure 12. Normalized Z-Component of Vorticity Contours, Outboard Data, Zero-Flap Deflection, Forward Station, $\bar{U}_t$ = 65.7 mph

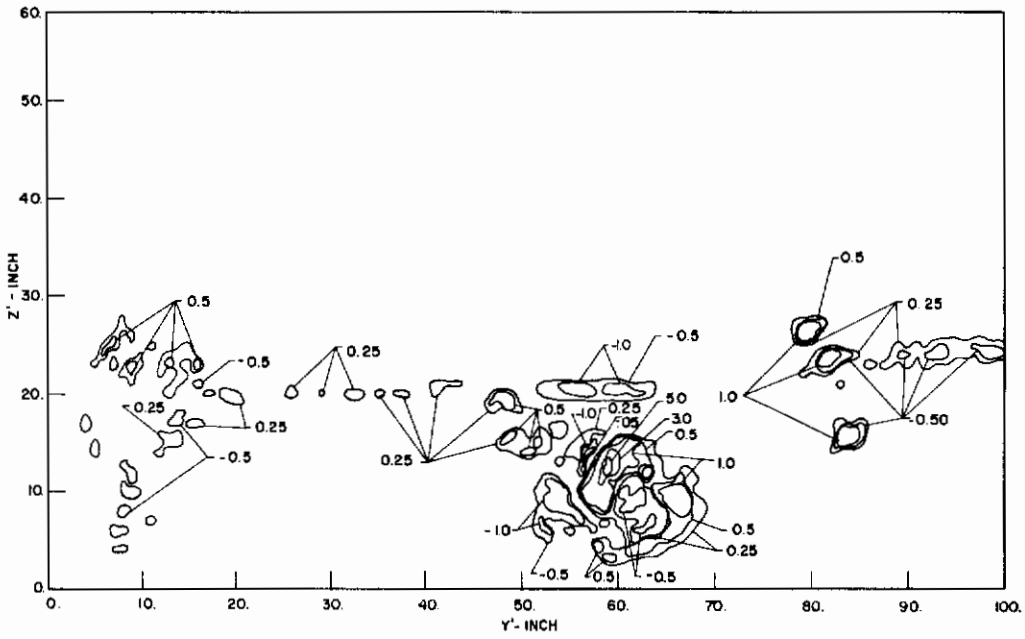

(A)

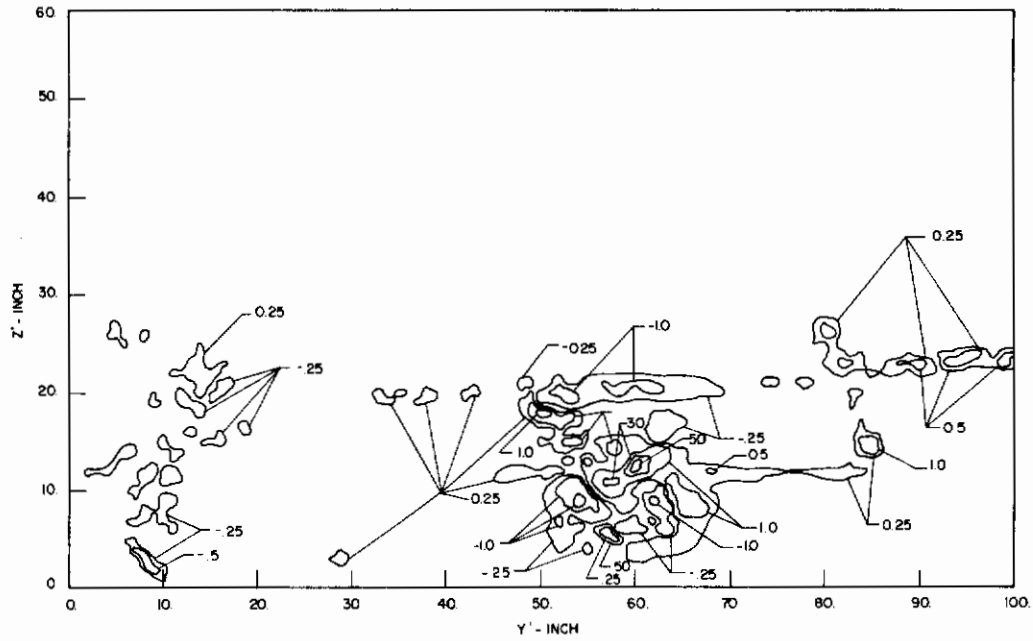

(B)

Figure 13. Normalized X-Component of Vorticity Contours, Inboard Data, Zero-Flap Deflection, (A) X = 5.1 inches, $\bar{U}_t$ = 65.5 mph, (B) X = 9.1 inches, $\bar{U}_t$ = 65.9 mph

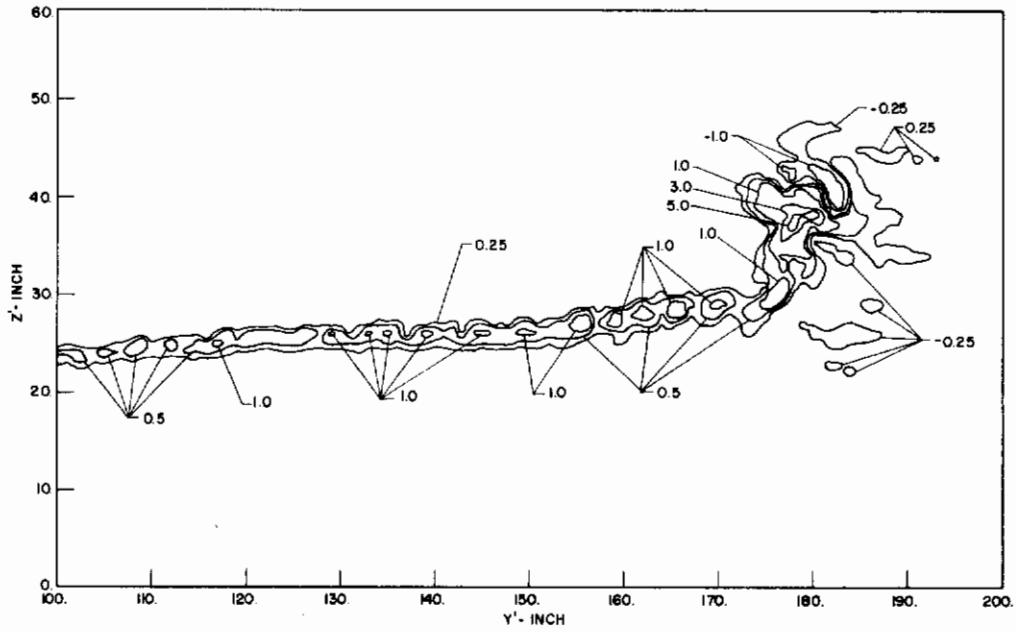

(A)

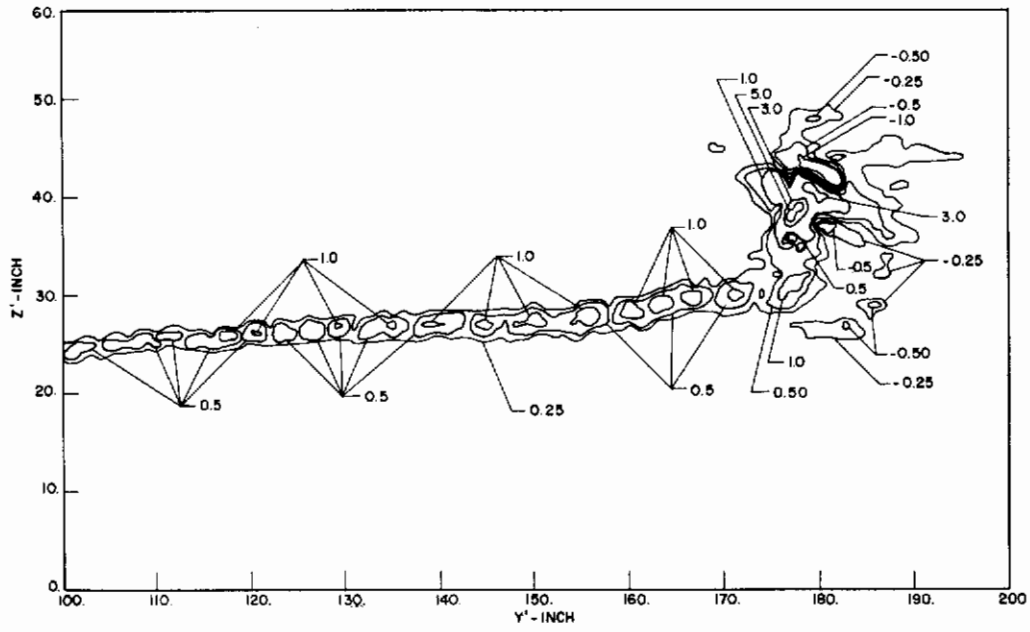

(B)

Figure 14. Normalized X-Component of Vorticity Contours, Outboard Data, Zero-Flap Deflection, (A) X = 5.1 inches, $\overline{U}_t$ = 65.5 mph, (B) X = 9.1 inches, $\overline{U}_t$ = 65.9 mph

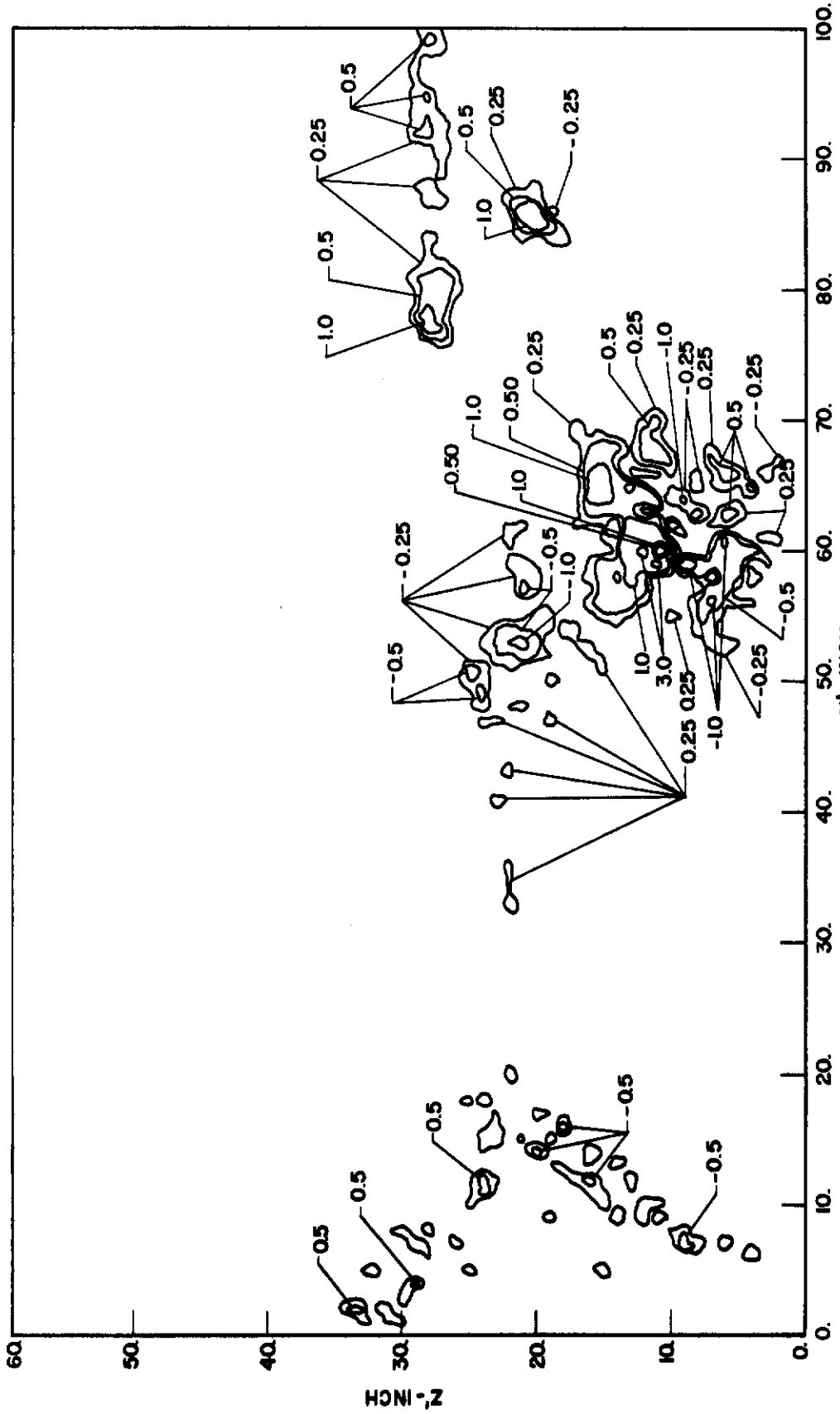

Figure 15. Normalized X-Component of Vorticity Contours, Inboard Data, Zero-Flap Deflection, Mid Station, $\bar{U}_t$ = 64.4 mph

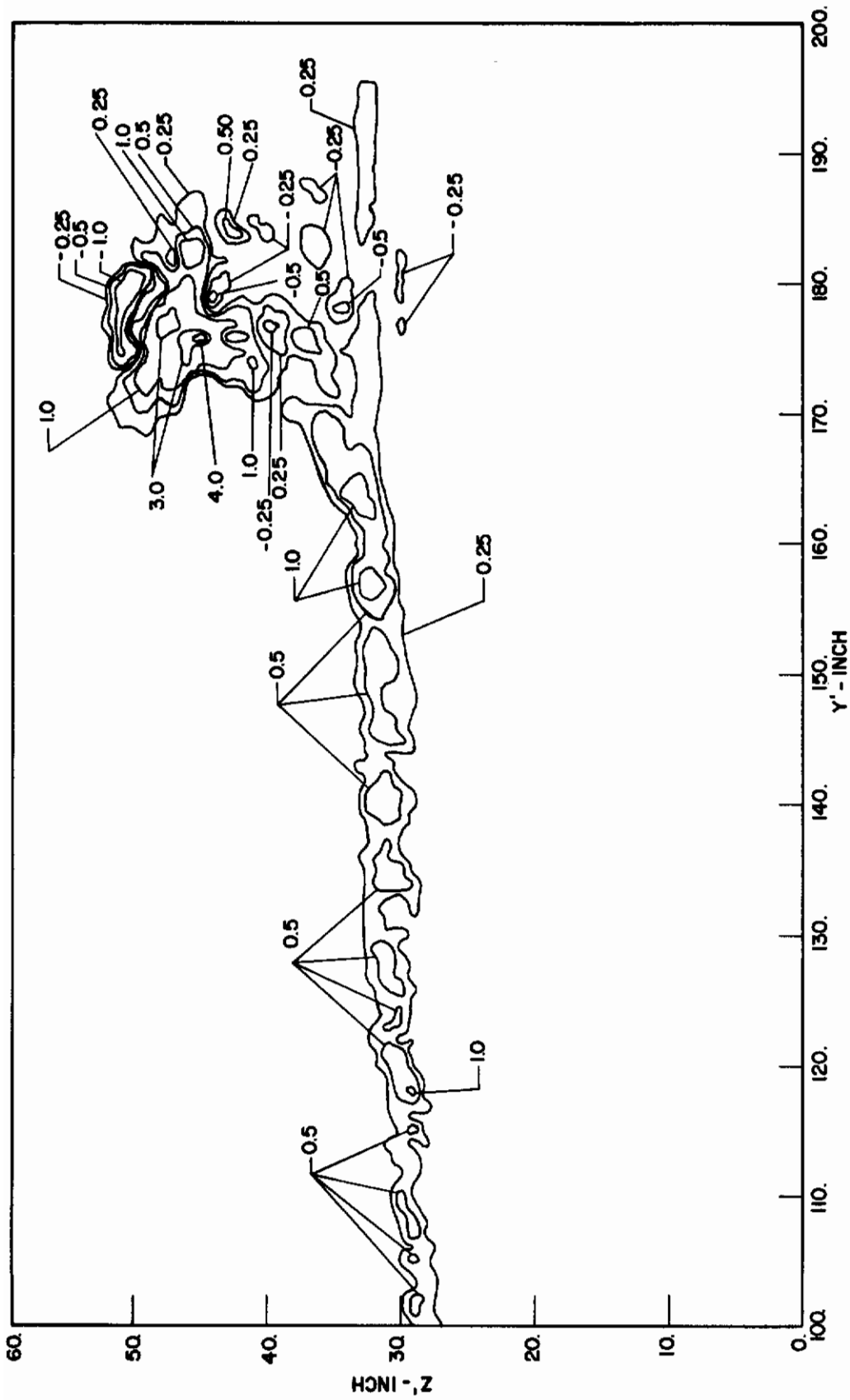

Figure 16. Normalized X-Component of Vorticity Contours, Outboard Data, Zero-Flap Deflection, Mid Station, $\bar{U}_t$ = 64.4 mph

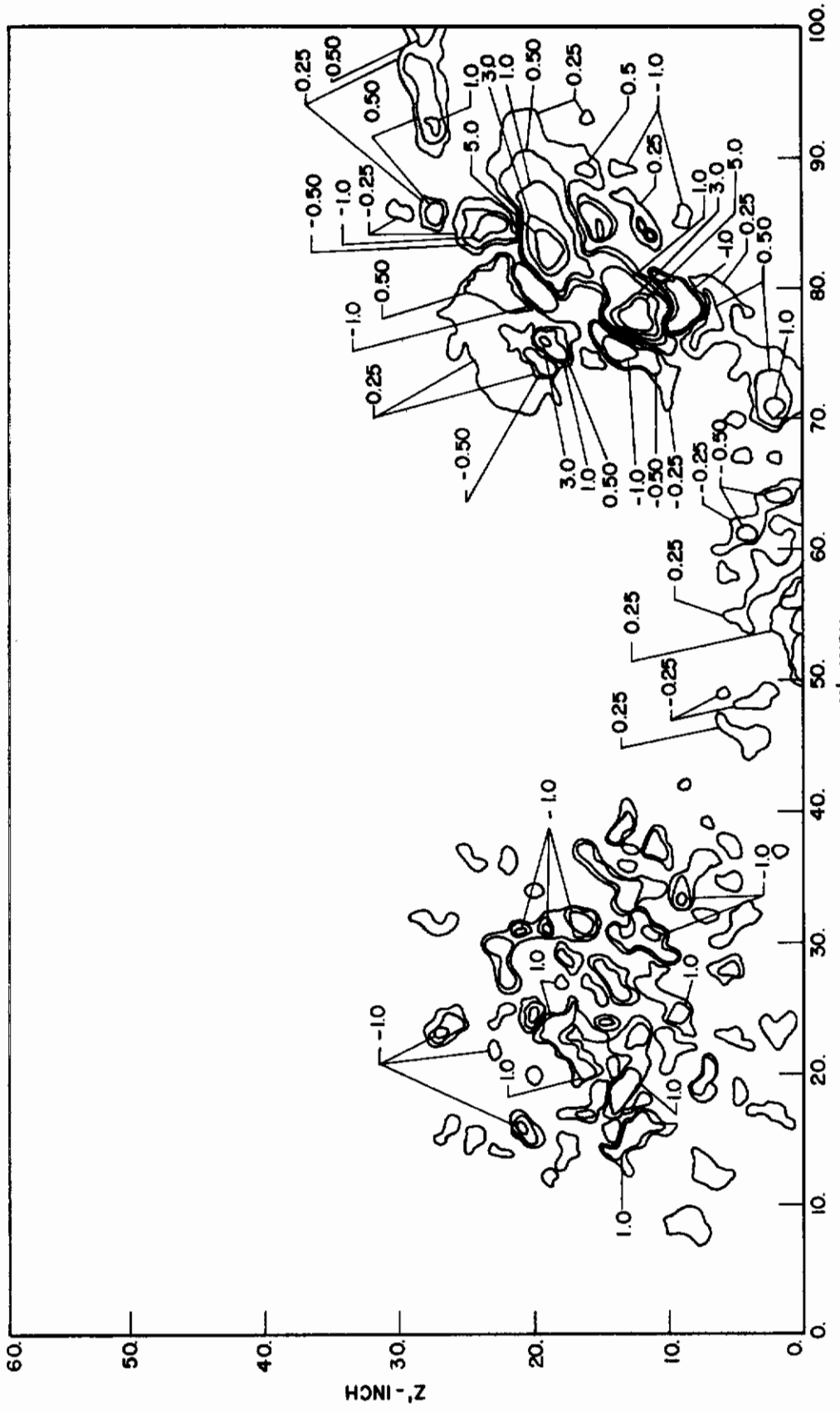

Figure 17. Normalized X-Component of Vorticity Contours, Inboard Data, Full-Flap Deflection, Mid Station, $\bar{U}_t$ = 64.8 mph

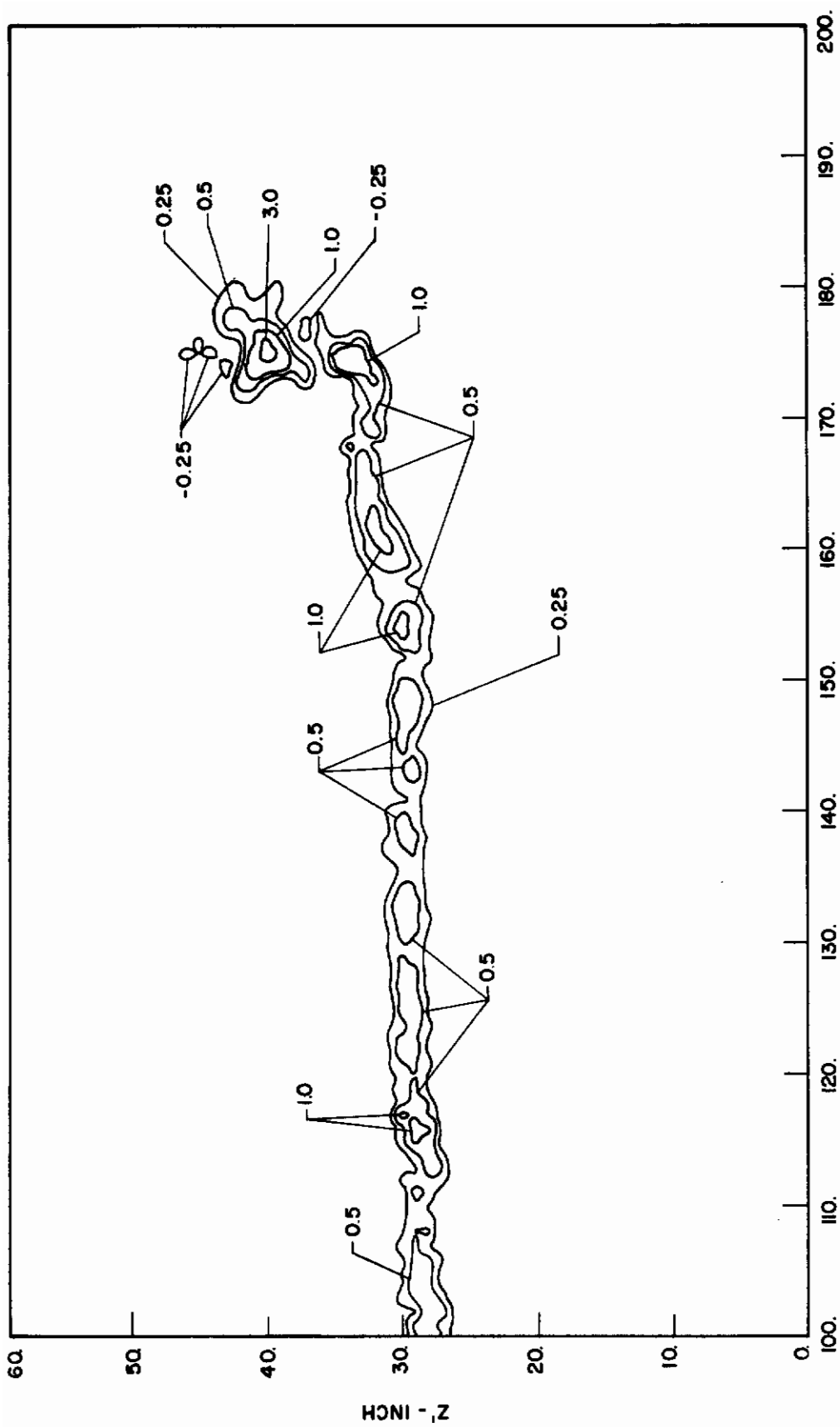

Figure 18. Normalized X-Component of Vorticity Contours, Outboard Data, Full-Flap Deflection, Mid-Station, $\bar{U}_t$ = 64.8 mph

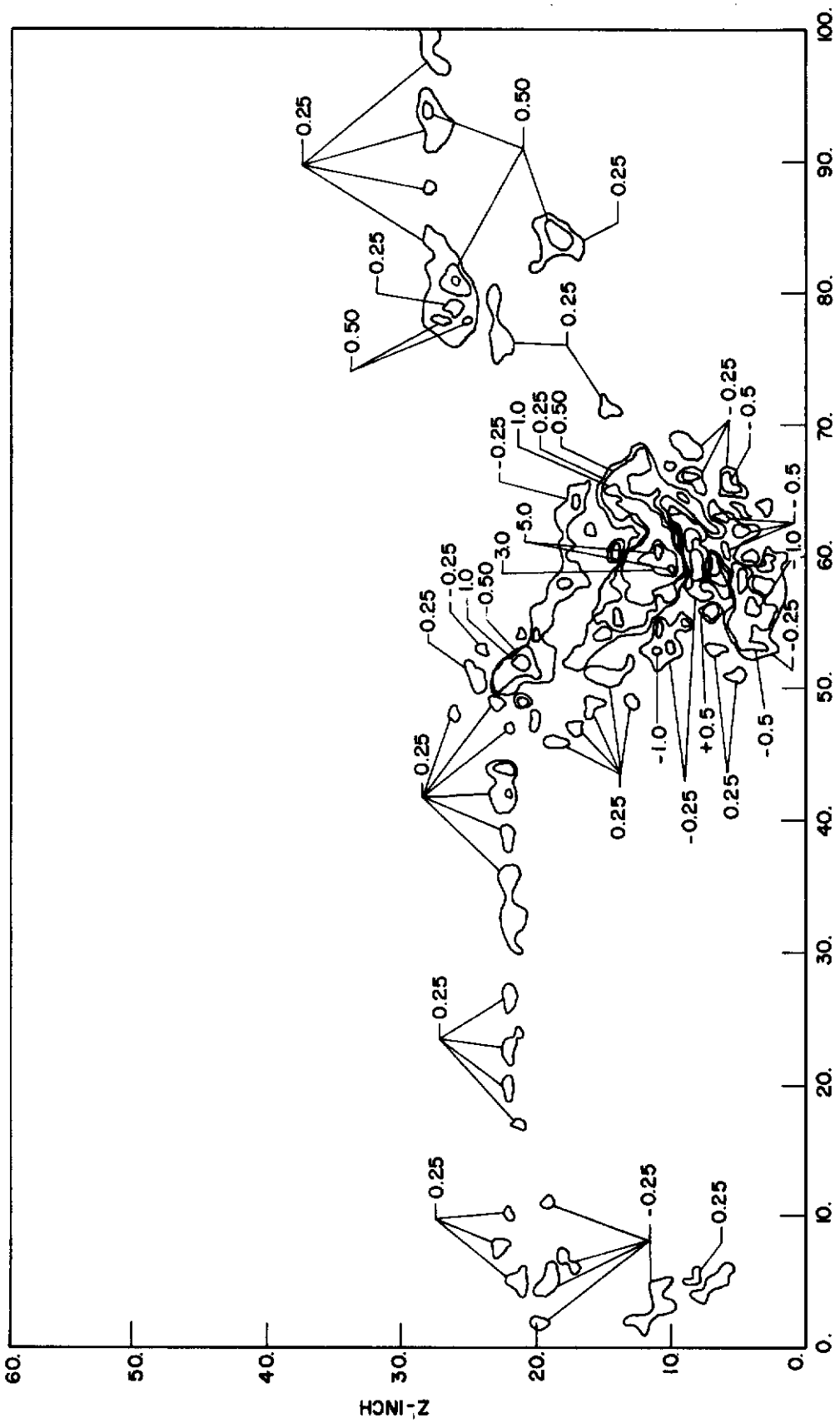

Figure 19. Normalized X-Component of Vorticity Contours, Inboard Data, Zero-Flap Deflection, Mid-Station, $\bar{U}_t$ = 85.3 mph

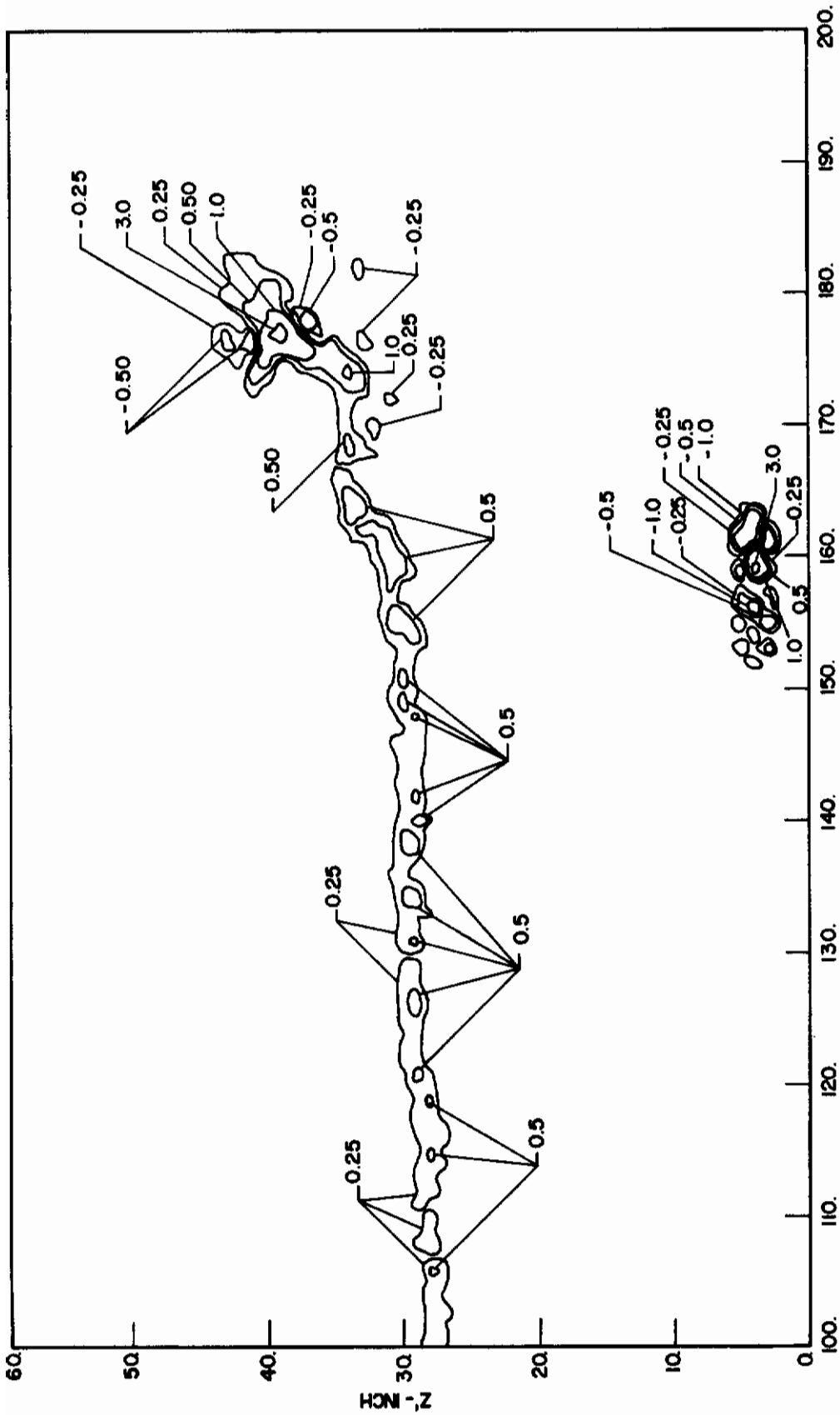

Figure 20. Normalized X-Component of Vorticity Contours, Outboard Data, Zero-Flap Deflection, Mid-Station, $\bar{U}_t$ = 85.3 mph

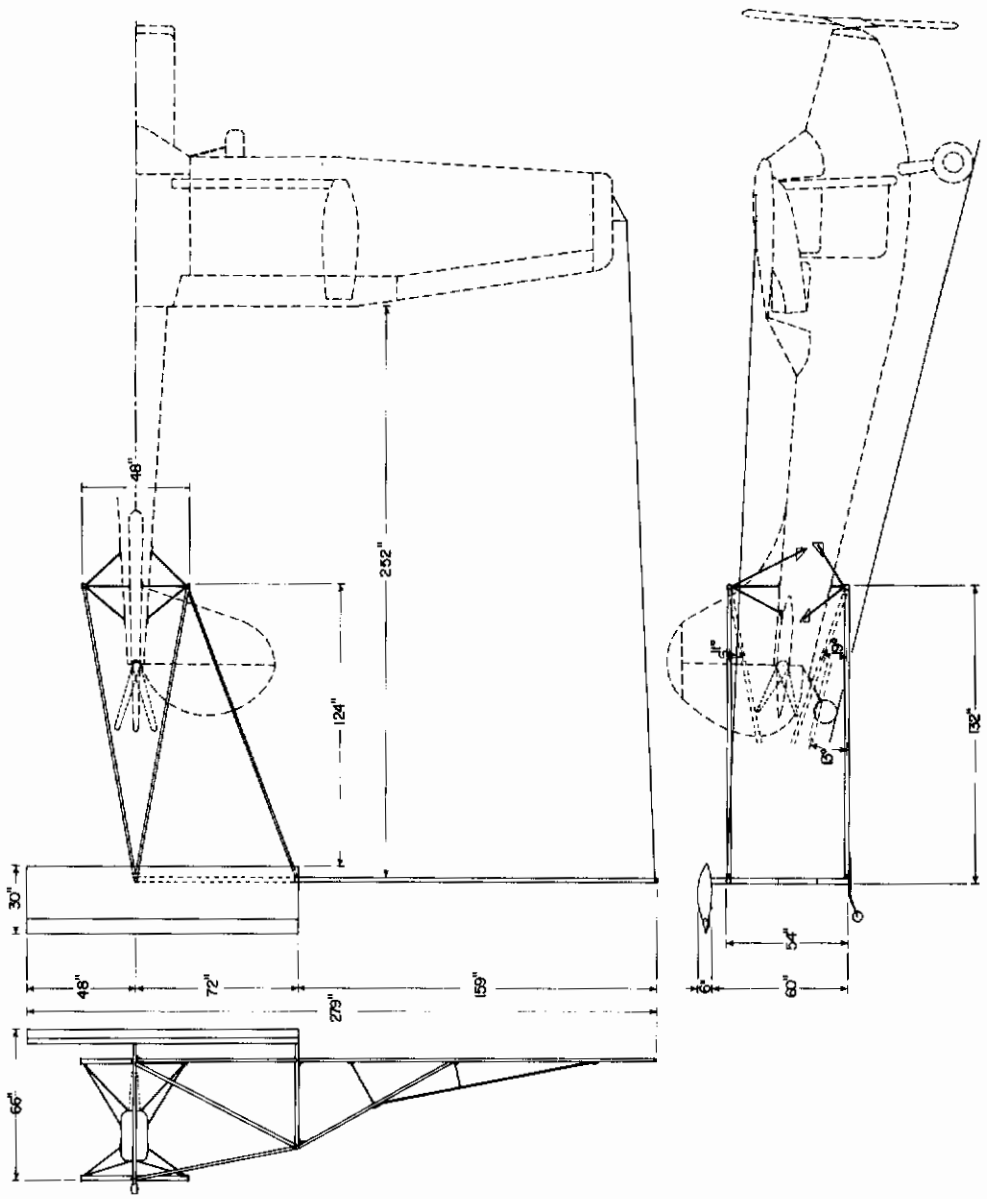

Figure 21. Trailing Boom Assembly 3-View Drawing

TABLE NO. 1 - STABILITY DERIVATIVES

DERIVATIVE	ABBREVIATION	NUMERICAL VALUE
C_ℓ	C_ℓ	0.2124
$\frac{\partial C_\ell}{\partial \alpha}$	C_{ℓ_α}	2.8863
$\frac{\partial C_\ell}{\partial \dot{\alpha}}$	$C_{\ell_{\dot{\alpha}}}$	0.2467
$\frac{\partial C_\ell}{\partial \dot{\theta}}$	$C_{\ell_{\dot{\theta}}}$	0.5960
$\frac{\partial C_\ell}{\partial \delta}$	C_{ℓ_δ}	0.0000
$\frac{\partial C_\ell}{\partial \dot{\delta}}$	$C_{\ell_{\dot{\delta}}}$	0.2818
$\frac{\partial C_M}{\partial \alpha}$	C_{M_α}	-1.6784
$\frac{\partial C_M}{\partial \dot{\alpha}}$	$C_{M_{\dot{\alpha}}}$	-0.0655
$\frac{\partial C_M}{\partial \dot{\theta}}$	$C_{M_{\dot{\theta}}}$	-0.1740
$\frac{\partial C_M}{\partial \delta}$	C_{M_δ}	0.0000
$\frac{\partial C_L}{\partial \alpha}$	a_w	4.9274
$\frac{\partial C_D}{\partial \alpha}$	C_{D_α}	0.3114

TABLE NO. 2. STABILITY CHARACTERISTICS

A. Airplane with Trailing Wing

MODE	PERIOD (SECS)	TIME TO DAMP TO HALF AMPLITUDE (SECS)
Long Period	23.60	16.88
Short Period 1	10.37	1.01
Short Period 2	1.58	0.25

B. Basic Airplane (Calculated)

MODE	PERIOD (SECS)	TIME TO DAMP TO HALF AMPLITUDE (SECS)
Long Period	21.92	38.90
Short Period	2.18	00.24

C. Basic Airplane (Flight-Test)

MODE	PERIOD (SECS)	TIME TO DAMP TO HALF AMPLITUDE (SECS)
Long Period	26.00	31.20
Short Period	Too small to be measured	

TABLE NO. 3. VARIATION OF STABILITY CHARACTERISTICS WITH MODIFICATION OF TRAILING WING PARAMETERS

MOD.	MODE	PERIOD (SECS)	TIME TO DAMP TO HALF AMPLITUDE (SECS)
Standard System	Long	23.60	16.88
	Short 1	10.37	1.01
	Short 2	1.58	0.25
w = 2w (Wt. of Trailing Wing System)	Long	29.68	15.78
	Short 1	10.27	2.63
	Short 2	1.74	0.27
w = w/2	Long	22.80	22.09
	Short 1	Very Large*	0.94
	Short 2	1.62	0.25
$S_t = 2S_t$	Long	23.03	14.96
	Short 1	Very Large	0.36
	Short 2	1.58	0.25
$S_t = S_t/2$	Long	24.12	17.33
	Short 1	11.13	2.09
	Short 2	1.58	0.25
$C_d = 2C_d$	Long	23.98	15.72
	Short 1	5.63	1.02
	Short 2	1.58	0.25
$C_d = C_d/2$	Long	22.57	16.45
	Short 1	Very Large	1.77
	Short 2	1.58	0.25

* Order of 10^{10}